Ocean Engineering 195 (2020) 106712

Contents lists available at ScienceDirect

Ocean Engineering

journal homepage: www.elsevier.com/locate/oceaneng

Review

A review on fluid dynamics of flapping foils

Xia Wu [a,b], Xiantao Zhang [a,b], Xinliang Tian [a,b,*], Xin Li [a,b], Wenyue Lu [a,b]

[a] State Key Laboratory of Ocean Engineering, Shanghai Jiao Tong University, Shanghai, 200240, China
[b] SJTU Yazhou Bay Institute of Deepsea Technology, Sanya, 572000, China

ARTICLE INFO

Keywords:
Flapping foil
Aerodynamics
Hydrodynamics
The law of parameter

ABSTRACT

The fluid dynamics of flapping foils are reviewed in this article. A very wide range of researches are conducted for the two-dimensional flapping foil which has a relatively simple geometry. However, for a three-dimensional foil, the aspect ratio and shape take effects and completely distinct fluid dynamics are revealed compared with the two-dimensional one. This review gives a summary on the experimental techniques and numerical methods used in the researches on the fluid dynamics of flapping foils. The effects of some key parameters including Reynolds number, reduced frequency, flapping amplitude and three-dimensional effect on the fluid dynamics of flapping foils are reviewed. The researches focusing on the wake structures, aero/hydrodynamic characteristics and energy harvesting efficiency are discussed. Finally, some conclusions are drawn and potential future research directions are recommended.

1. Introduction

Oscillating foils are very common in nature and human activities. For instance, birds need to flap their wings to produce lift and thrust so that they can hover and locomote in the air; fishes take advantage of the flapping motion of their pectoral and caudal fins to achieve optimal propulsion. These aquatic and flying animals acquire highly effective fluid dynamic performance via their own oscillatory motion of fins or wings. Through taking an insight into these curious phenomena, many experts and scholars have grasped some crucial principles which can be applied into engineering area by performing a variety of experiments and numerical simulations. Firstly, Birnbaum (1924a, b) reported that a flapping wing could be used as a novel propeller. Since then, various types of device which utilize the flapping motion of foils or wings for different purposes have been proposed, such as wave gliders whose propulsion force is provided by tandem hydrofoils in unsteady flows (Wang et al., 2019) and ocean energy harvesting device which makes use of flapping foils to extract energy from wind, wave or current (Xu and Sun, 2016; Chen et al., 2017), while rotary wind and water turbines are still dominant in renewable energy area (Guo et al., 2017a,b; 2018a, b; Wen et al., 2017a,b; 2018a,b). As one of the hot topics in the field of fluid mechanics, the fluid dynamics of flapping foil has been investigated over several decades and hundreds of papers were published. Fig. 1 summarizes almost 400 papers with relatively high citation frequency on flapping foils published since 1970. It is obvious that the number of papers before 2000 was small while a dramatic increase happened after that, which reveals the heat of studies on flapping foils are unprecedentedly high in recent years.

The research activities about the flapping foil distribute widely around the world and come from more than 20 countries across different continents. Fig. 2 reveals that the numbers of articles from USA and China take up a proportion of 40.21% and 16.49% respectively. The major sources of papers are from Massachusetts Institute of Technology, Naval Postgraduate School, Princeton University and New York University in USA while Chinese papers mainly come from Xi'an Jiao Tong University, Zhejiang University, Chinese Academy of Sciences, Nanjing University of Aeronautics and Astronautics and University of Science and Technology of China etc. The proportion taken up by Australia, UK and France is between 5% and 10% and the rest of countries are no more than 5%. It is noteworthy that a portion of papers are authored (or collaborated) by people from two or more countries.

Some efforts have also been taken on utilizing flapping foils as ship propulsion. The researchers from National Technical University of Athens (NTUA) carried out many numerical works on this issue (Belibassakis et al., 1997; Belibassakis, 2011; Belibassakis and Politis, 2013; Belibassakis and Filippas, 2015; Filippas et al., 2018; Politis, 2004; Politis and Tsarsitalidis, 2009, 2013; 2014; Politis and Politis, 2014; Tsarsitalidis and Politis, 2015). They numerically investigated the hydrodynamic performance of flapping foils for ship propulsion under different conditions using the Unsteady Boundary Element Modeling

* Corresponding author. State Key Laboratory of Ocean Engineering, Shanghai Jiao Tong University, Shanghai, 200240, China.
E-mail address: tianxinliang@sjtu.edu.cn (X. Tian).

https://doi.org/10.1016/j.oceaneng.2019.106712
Received 28 February 2019; Received in revised form 28 September 2019; Accepted 10 November 2019
Available online 28 November 2019

code UBEM (Politis, 2009, 2011). Almost all results show that compared to conventional propellers, flapping foils can be a promising system with better propulsion efficiency and energy extraction from ship motion. Furthermore, Bøckmann and Steen from Norwegian University of Science and Technology (NTNU) performed experimental investigation on the effect of fixed wavefoils on ship motion and propulsion (Bøckmann and Steen, 2013, 2016), and the effect of control methods of oscillating motion on performance of foils (Bøckmann and Steen, 2014). They concluded that both ship resistance and motion were reduced by the wavefoils and oscillating foils can be acted as a major or auxiliary driving force of ship. In addition, Thaweewat et al. (2018) studied the performance of semi-active flapping foil for ship propulsion. Similar investigations were also conducted by Liu et al. (2019), Bøckmann and Steen (2014), Belibassakis and Filippas (2015) and Filippas et al. (2018). Floc'h et al. (2012) performed a comparison between a porpoising foil as propulsion and a conventional propeller. Results indicated that the two propulsion systems had the similar hydrodynamic performance despite their different nature. Based on these numerical and experimental work, some practical applications have been realized in the realm of ocean engineering. MARIN has built the first inland ship with O-foil (oscillating foil) propulsion, resulting in 50% better efficiency and a cut in fuel consumption by 33% till 50% in comparison with the screw propeller. The project of Unmanned Surface Vessel (USV) called AutoNaut developed a novel vessel propelled forward by four keel-mounted foils converting energy from the pitch and roll of the waves. Biomimetic propulsors has many advantages with aspect of economy, environment and efficiency etc. and thus they need to be investigated intensively so that ship propulsion based on flapping foils can be used more widely.

The model of oscillating foil can be simplified into a two-dimensional object with an airfoil section oscillating in the fluid. As a result, early researches were conducted on the two-dimensional problems both theoretically and experimentally, focusing on the force (drag, lift and thrust), moment and propulsion generated by oscillating foils (Knoller, 1909; Betz, 1912; Katzmayr, 1922; GIauert, 1929; Garrick, 1936; Koochesfahani, 1989; Dohring et al., 1996). Knoller (1909) and Betz (1912) firstly adopted a flapping wing to explain the mechanism of thrust generation, which represents the beginning of the researches on flapping foils. Subsequently, Katzmayr (1922) verified the Knoller-Betz effect and this is the first time to validate this phenomenon with experimental method. Onset of the two-dimensional flow visualization structure arising from flapping motion was addressed early from the experiments in the 20th century (von Kármán and Burgers, 1943; Bratt, 1950; Wood and Kirmani, 1970; Freymuth, 1988, 1990; Koochesfahani, 1989). von Kármán and Burgers (1943) firstly explained the production of drag and thrust theoretically by observing the wake structure. Bratt (1950) confirmed von Kármán and Burgers's explanation through flow visualization experiments. Freymuth (1988) presented the visualization on the propulsive vortical signature of two-dimensional airfoils with pure plunging and pure pitching motion. Koochesfahani (1989) performed the flow visualization on vortical patterns of a pitching airfoil with nonsinusoidal oscillations. Soap film tunnels are the simple and efficient flow visualization tools to observe various vortex flows (Couder and Basdevant, 1986; Gharib and Derango, 1989; Rivera et al., 1998; Zhang et al., 2000; Schnipper et al., 2009; Andersen et al., 2017). Further, vortex formation is found to be different under different flow conditions. It is mainly dependent on the parameters including amplitude and frequency which also influence thrust and lift generation of a flapping foil. Until recently, the issues of a two-dimensional foil are still being studied. Andersen et al. (2017) and Schnipper et al. (2009) performed numerical simulation with experimental verification of a two-dimensional foil with pure heaving and pure pitching respectively. They concluded that these two modes of motion are essentially the same from their wake map. Smits' team mainly focus on the scaling law between geometric, kinematic and environmental parameters and thrust, power and energy consumption of an oscillating foil (Dewey et al., 2011, 2013; Moored et al., 2012; Quinn et al., 2015; Buren et al., 2017, 2018; Floryan et al., 2017, 2018). Peng et al. (2018a, b) studied the collective locomotion of two and multiple self-propelled plates (two-dimensional) in different configurations and they found four typical locomotion states and two schooling states respectively. Although an oscillating foil can be simplified into a two-dimensional foil and studied for such a long time, the physical mechanism involved is still unclear in some aspects.

The real foil always has a limited aspect ratio and thus the three-dimensional flow structure can be generated due to the end effect. Taira and Colonius (2009) used direct numerical simulations (DNS) to study the wake structures of rectangular plates with different aspect ratios and non-rectangular plates under the state of inclination. Soria's team performed experiments to discuss the effect of amplitude and frequency of an oscillating finite-span wing on three-dimensional vortex structure at low Reynolds number (von Ellenrieder et al., 2001; von Ellenrieder et al., 2002; von Ellenrieder et al., 2003; Parker et al., 2007). Except for rectangular plate, there are many researches on oscillating plates of other shapes, such as the circular disk (Yang et al., 2014; Tian et al. 2017a,b), the elliptic disk (Dong et al., 2006; Yilmaz and Rockwell, 2012; Harbig et al., 2013; Wang et al., 2016a) and the trapezoidal plate (Green et al., 2011). However, Zhang (2017) specially pointed out that the problems on how to make an oscillating foil generate maximum thrust and have energy harvesting efficiency up to the optimal state are still unclear. Hence two main conundrums are presented: (i) how to systematically and accurately understand the complex flow mechanism around the three-dimensional oscillating aero/hydro-foil. (ii) how to achieve the high efficient control of the three-dimensional oscillating aero/hydro-foil to optimize propulsion and energy harvesting performance. Once both of them are solved, application of the oscillating foil

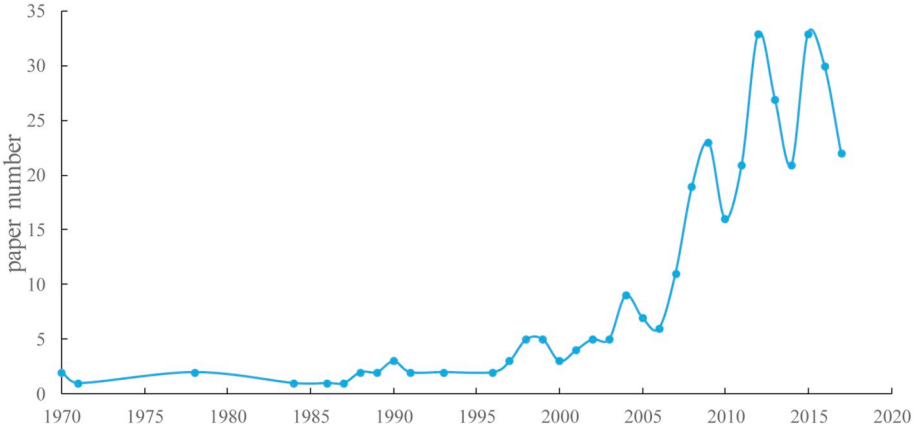

Fig. 1. The number of papers on flapping foils since 1970.

will be promoted in the field of propulsion and current/wind energy harvesting devices. It is the reason that the studies of flow structure and aero/hydrodynamic performance and the researches on how to enhance propulsive efficiency and energy harvesting efficiency have always been the research hotspots and continue to increase recently, as indicated in Fig. 3(b). The improvements from these researches are important for some engineering applications. Based on the in-depth study of flapping foils, it is found that the effects of Reynolds number, three-dimensional effect, foil flexibility and other parameters on aero/hydro-dynamic performances including thrust, lift and propulsion efficiency are not 'an easy issue'.

This review aims to provide a comprehensive summary on the researches about the aero/hydro-dynamics of flapping foils and then give some directions for the future work on this topic. The remainder of this paper is organized as follows. A brief description for the problem of the foil is given in Section 2, including parameter description, motion mode and research contents. Experimental techniques used to record the force and flow structure in experiments and various numerical simulation methods adopted in numerical studies are summarized in Section 3. Some key results arising from the change of some significant parameters, which are the most crucial portion and of a considerable practical significance, are addressed in Section 4. Finally, summary and outlook are drawn in Section 5.

2. Problem description

2.1. Governing parameters

It is easy to have the false impression that a flapping foil in fluid is a simple problem. However, it is true that more than 10 governing parameters have been mentioned in the articles reviewed here. These parameters can be divided into four types: environmental parameter (describing the fluid properties), geometric parameter (describing the shape of foils), kinematic parameter (describing the motion of foils) and performance parameter (describing propulsion and energy harvesting performance of foils). The number of parameters involved in a single paper is normally not limited to one. Schematics of some parameters are described in Figs. 4 and 5.

2.1.1. Environmental parameters

There are many parameters about fluid properties but only a few of them are normally considered when it comes to the flapping foils. Freestream velocity U_∞, kinematic viscosity ν of the fluid as well as Reynolds number Re defined by both of them are the dominant parameters considered in the researches of flapping foils. The Reynolds number is defined as

$$Re = \frac{U_\infty L_0}{\nu} \tag{1}$$

where L_0 is the characteristic length which may be represented by the chord length c, the maximum thickness D or span length L (aiming at three-dimensional issues) of the flapping foil. The corresponding Reynolds number Re is defined, respectively, as

$$Re_c = \frac{U_\infty c}{\nu}, \quad Re_D = \frac{U_\infty D}{\nu}, \quad Re_L = \frac{U_\infty L}{\nu} \tag{2}$$

Specially, Shinde and Arakeri (2013) investigated the jet generated by a NACA0015 foil pitching in quiescent fluid where U_∞ is zero. Re is defined as

$$Re_{TE} = \frac{V_{TE_{\max}} c}{\nu} \tag{3}$$

where $V_{TE_{\max}}$ is the maximum velocity of trailing edge (TE). Although Mach number Ma is another key parameter in the high speed air flow, its effect on flapping foils is rarely mentioned.

2.1.2. Geometric parameters

The parameters determining the shape of a foil include the chord length c, the maximum thickness D, the span length L, the cross-section shape and the planform, as shown in Fig. 4. For the so-called two-dimensional (2D) foil, only c, D and the cross-section shape are considered. The cross-section shape is normally rectangle, ellipse and teardrop, among which teardrop is the most studied one. Generally, some teardrop-shaped foils are defined as a proprietary name, such as NACA series, SD series, EPPLER series and SG series. Based on the two-dimensional foil, L is added to describe a foil but its value is infinite, which is so-called the 'pseudo three-dimensional' foil. In fact, such issues still focus on two dimensions and do not take three-dimensional effect into consideration. However, when the value of L is finite, the foil is the so-called 'true three-dimensional (3D)' foil. The planform is mainly circle, ellipse, triangle, trapezoid and rectangle, among which rectangle is the most studied one. Hence, aspect ratio (AR) is introduced and defined as

$$AR = \frac{L}{c} \tag{4}$$

The effects of AR on the three-dimensional flapping foil have been presented briefly in Section 1. In addition, another parameter that

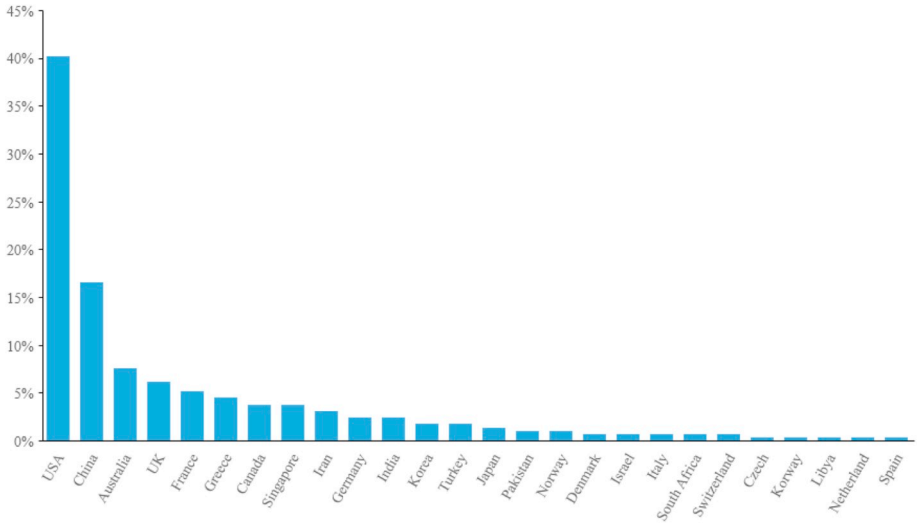

Fig. 2. The proportional statistics on paper numbers based on the author's affiliated institute.

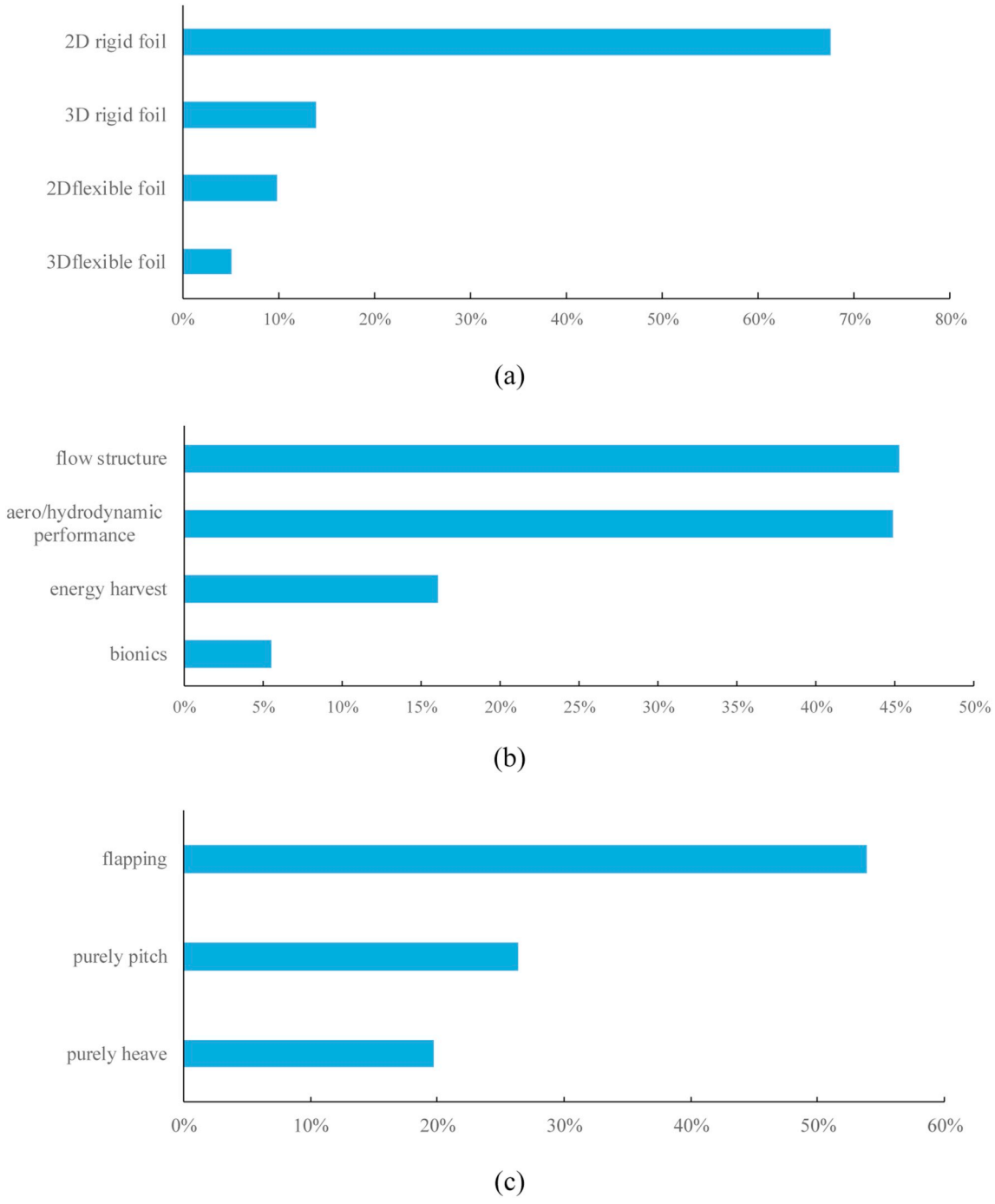

Fig. 3. The proportional statistics of (a) research object, (b) research content and (c) motion mode of the foil.

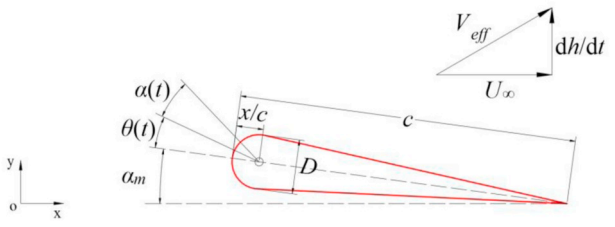

Fig. 4. Schematic of foil kinematic parameters, showing the relationship between physical pitch angle, effective angle of attack and mean angle of attack. dh/dt denotes heave velocity and V_{eff} denotes the relative velocity vector between the incoming flow and the flapping foil.

should be introduced is the flexibility of foil. The shape of foil will change constantly with its flapping motion. Researches on flexible foils (both 2D and 3D) account for almost 15% as shown in Fig. 3(a). Dewey et al. (2013) pointed out that the thrust of the flexible oscillating foil can be increased by 1–2 times and the propulsion efficiency can be doubled. Cleaver et al. (2016) demonstrated that the flexibility of the oscillating foil enlarges the motion amplitude, which increases the lift force significantly. Moreover, investigations on energy harvesting devices based on flexible foils were conducted numerically (Zhu et al., 2009; Griffith et al., 2016; Liu et al., 2016). It is necessary and important to give an accurate description of foil geometry, which is the basis of all researches.

Most studies are conducted on the 2D foil (including the infinite foil)

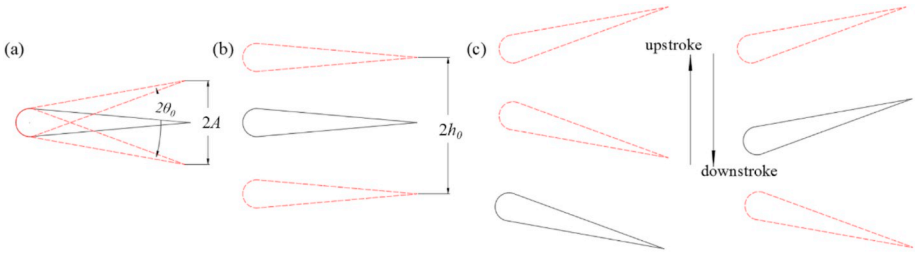

Fig. 5. Schematics of (a) pitching motion, (b) heaving motion and (c) flapping motion of a foil.

because they have the advantages of simple problem, clear physics, easy mathematical description, simple numerical simulation and so on. A large number of researches mainly concentrate on a 2D foil which take up almost 78%. Nevertheless, three-dimensional effect is unavoidable in nature and the 2D foil cannot reflect its true physical mechanism in many conditions. As a result, more and more issues have been investigated based on 3D.

2.1.3. Kinematic parameters

The oscillation motion of a foil is characterized by several parameters. Firstly, the Strouhal number St, describing the externally imposed frequency, is defined as

$$St = \frac{f\ L_0}{U_\infty} \tag{5}$$

where f is the frequency of the oscillation. Similar to the definition of Re, St can be defined as

$$St_c = \frac{f\ c}{U_\infty},\quad St_D = \frac{f\ D}{U_\infty},\quad St_A = \frac{f\ A}{U_\infty} \tag{6}$$

where A is peak-to-peak amplitude as shown in Fig. 5, St_c, St_D and St_A are the chord-based, the maximum thickness-based and amplitude-based Strouhal number, respectively. When the flapping amplitude is defined in length as A or h_0 (heave or plunge amplitude, respectively), the dimensionless amplitude can be often defined as

$$A_D = \frac{A}{D}, A_c = \frac{A}{c}. \tag{7}$$

$$h = \frac{h_0}{c} \tag{8}$$

Particularly, St_A is equal to the product of St_D and A_D. It can be treated as the ratio between the oscillation velocity of the foil trailing edge and the freestream velocity. St_A is often used as a criterion for describing drag-thrust transition (Triantafyllou et al., 1991). As we know, the fish-like swimming and flapping flight in nature occur for St_A = 0.2–0.4, the specific reason of which is still unclear. Reduced frequency is another frequently used non-dimensional form of oscillating frequency, defined as

$$k = \frac{\omega c}{U_\infty} = \frac{2\pi fc}{2U_\infty}. \tag{9}$$

Flapping foil motion is designed to couple two sinusoidal motions with the same frequency in the most literatures, which are respectively defined by

$$h(t) = h_0 \sin(2\pi ft) \tag{10}$$

$$\theta(t) = \theta_0 \sin(2\pi ft + \phi) \tag{11}$$

where θ_0 is the pitch amplitude, $h(t)$ is the instantaneous vertical position of the foil axis, $\theta(t)$ is the instantaneous angle between the freestream velocity U_∞ and the foil chord and ϕ is the phase angle between pitch and heave. Noteworthily, effective (instantaneous) angle of attack α_{eff} is calculated with three terms as following

$$\alpha_{eff} = \alpha_m + \theta_0 \sin(2\pi ft + \phi) - \tan^{-1}\left[\frac{h_0 2\pi f \cos(2\pi ft)}{U_\infty}\right] \tag{12}$$

where α_m is the mean angle of attack (or geometric angle of attack). When reaching the maximum angle, α_{eff} is the so-called nominal effective angle of attack α_0. Specially, with $\phi = 90°$, the maximum (nominal) angle of attack becomes

$$\alpha_{\max,eff}(\alpha_0) = \alpha_m + \theta_0 - \tan^{-1}\left(\frac{h_0 2\pi f}{U_\infty}\right) \tag{13}$$

In some literatures, pitch amplitude θ_0 is not given but nominal angle of attack α_0 is used as an alternative parameter.

Pivot location of the foil is based on the chord length c as shown in Fig. 4. The leading edge of chordwise and the root of spanwise are special location. Moreover, angle of attack profile selected in most experiments and simulations is sinusoidal which means that both of pitch and heave motion are sinusoidal. Similarly, variable pivot location and non-sinusoidal motion can also change the motion of the foil and influence the flow structures and hydrodynamic forces of the foil.

2.1.4. Performance parameters

The parameters describing the propulsion performance of an oscillating foil includes thrust coefficient C_T, input power coefficient C_p and propulsion efficiency η. The mean thrust coefficient is defined as

$$\overline{C_T} = \frac{\overline{F_x}}{0.5\rho U_\infty^2 cL} \tag{14}$$

where ρ is the fluid density and $\overline{F_x}$ is the time-averaged force in x direction, defined as

$$\overline{F_x} = \frac{1}{\tau}\int_0^\tau F_x(t)\mathrm{d}t \tag{15}$$

where $F_x(t)$ is the instantaneous force component in x direction and τ is the oscillation period. The mean input power coefficient $\overline{C_P}$ is defined as

$$\overline{C_P} = \frac{\overline{P}}{0.5\rho U_\infty^3 cL} \tag{16}$$

where $\overline{P}$ is mean input power, calculated by

$$\overline{P} = \frac{1}{\tau}\left[\int_0^\tau F_y(t)\frac{\mathrm{d}h(t)}{\mathrm{d}t}\mathrm{d}t + \int_0^\tau M_\theta(t)\frac{\mathrm{d}\theta(t)}{\mathrm{d}t}\mathrm{d}t\right] \tag{17}$$

where $F_y(t)$ is the instantaneous force component in y direction, $M_\theta(t)$ is the instantaneous pitching moment and $\mathrm{d}h/\mathrm{d}t$ and $\mathrm{d}\theta/\mathrm{d}t$ are derivatives of heave and pitch motion, respectively. The final propulsion efficiency is expressed as

$$\eta = \frac{\overline{C_T}}{\overline{C_P}} \tag{18}$$

The key parameters describing the energy harvesting efficiency of an oscillating foil are output power coefficient C_{op} and the energy

harvesting efficiency η_{op}. The mean output power coefficient is defined as

$$\overline{C_{op}} = \frac{\overline{P_o}}{0.5\rho U_\infty^3 cL} = \overline{C_{opy}} + \overline{C_{op\theta}} = \frac{1}{\tau}\left[\int_0^\tau C_y \frac{\mathrm{d}h(t)}{\mathrm{d}t}\mathrm{d}t + \int_0^\tau c \cdot C_m \frac{\mathrm{d}\theta(t)}{\mathrm{d}t}\mathrm{d}t\right] \quad (19)$$

where $\overline{P_o}$ is the mean output power, $\overline{C_{opy}}$ is the mean power coefficient of heaving motion and $\overline{C_{op\theta}}$ is the mean power coefficient of pitching motion. C_y is the instantaneous heave force coefficient and C_m is the instantaneous pitching moment coefficient, defined as

$$C_y = \frac{F_y}{0.5\rho U_\infty^2 cL} \quad (20)$$

$$C_m = \frac{M_\theta}{0.5\rho U_\infty^2 c^2 L} \quad (21)$$

The energy harvesting efficiency is expressed as

$$\eta_{op} = \frac{\overline{P_o}}{0.5\rho U_\infty^3 dL} = \overline{C_{op}}\frac{c}{d} \quad (22)$$

where d is the maximum vertical displacement of the trailing edge of the flapping foil.

It must be noted that, the parameters related to propulsion efficiency are under the condition of an oscillating foil with combined pitching and heaving motion, and the parameters related to energy harvesting efficiency are under the condition of a harvest device with forced pitching and heaving motion. Moreover, Xiao and Zhu (2014) have made a thorough review on the energy harvesters based on foils and the definitions for energy harvesting efficiency of three types of flapping foil flow energy harvesters have been introduced in detail.

2.2. Motion mode of the foil

The motion mode of a foil has a crucial effect on the wake structure and aero/hydrodynamic performance of a flapping foil. The motion mode can be classified into three categories: plunging (or heaving), pitching and flapping, among which flapping is the combination of plunging and pitching. These motion can also be of full-active motion, semi-active motion or full-passive motion. The schematics of them are shown in Figs. 5 and 6. Full-active motion means that both pitching motion $\theta(t)$ and heaving motion $h(t)$ are prescribed and it is widely considered for oscillating foils. The systems with forced pitching and induced heaving motions, and self-sustained pitching and heaving motions are called semi-activated systems and full-passive systems, respectively. Both are the typical models for issues on flow energy harvesters based on flapping foils. For semi-active (semi-passive) system, it also can be composed of forced heaving and induced pitching motion. Boudreau et al. (2019a, b) numerically proved that the novel semi-passive flapping-foil turbine with a prescribed heave motion and a passive pitch motion can achieve the similar performance with fully-active flapping-foil turbine. Moreover, Bøckmann and Steen (2014) experimentally concluded that a passive pitching and forced heaving foil can produce higher thrust than that of the fully-constrained foil. However, Tsarsitalidis and Politis (2015) found that the contributions of a heaving wing, pitching passively (spring loaded) as energy harvester is more than that as main propulsion device. These results show that the foil with semi-passive motion have a great potential in terms of energy harvesting. Boudreau et al. (2018, 2020) and Duarte et al. (2019) discussed the dynamic behavior of the full-passive flapping foil turbine numerically and experimentally, respectively. Fig. 3(c) reveals the proportional distribution of three mentioned motion modes. Compared to pure heaving and pure pitching motion, research on flapping motion attracts more attentions whose proportion is almost 54%.

2.3. Research contents

Researches on flapping foil began in the 20th century, the content of which includes four main aspects, namely: aero/hydro-dynamic performance, energy harvesting, flow structure and bionics. The proportion of them are presented in Fig. 3(b). The researches on aero/hydrodynamic performance and flow structure whose proportion are 44.89% and 45.26% respectively, far more than the other two. Aero/hydrodynamic performance mainly focuses on the lift, drag, thrust generation and propulsion efficiency thereby achieving optimal performance. How to improve performance is still a key issue until now because great performance contributes to the engineering applications. The flow structures around the foil have been investigated and help to explain the complex flow mechanism. Actually, flow structure directly determines the aero/hydro-dynamic force so researchers normally explain force generation of the oscillating foil through the analysis of flow structures. The issues of energy harvesting efficiency arise from anxious desires and needs for renewable energy. Its basic principle is that energy harvester extracts energy from the flow and converts it into the electricity for human. Therefore, how to design and control the energy harvester devices is a crucial direction that needs to be continuously broken through. So the recent investigations and attention of energy harvesting based on flapping foils present a gradually increasing trend. Bionics based on the oscillating foil is a study on the locomotion of aquatic and flying animals through numerical and experimental methods. The model of the caudal fin of fish and the wing of birds are designed for researches to imitate fish-like swimming and flapping-like flying. Gursul and Ho (1992) found that unsteady motion of the foil creates very high lift coefficient. Esfahani et al. (2013) concluded that the propulsive efficiency could be enhanced in fish-like swimming which is more efficient than that of flapping-wing flying. Although the study of bio-inspired motion takes up the least number with respect to the rest three aspects, it seeks to draw accurate conclusion about condition of generating optimal thrust, lift or propulsion efficiency from the locomotion of aquatic and flying animals to apply to engineering area. Biomimetic propulsors are gradually developed for marine propulsion due to its friendliness to environment and considerable efficiency. The applications of horizontal and vertical foils and wings mounted on different locations of the ship are benefit for ship stabilization and additional thrust and energy can be obtained owing to the pitching and heaving motion of foils induced by the ship responses (Bøckmann and Steen, 2013, 2016; Belibassakis and Filippas, 2015; Belibassakis and Politis, 2013; Politis and Tsarsitalidis, 2014; Tsarsitalidis and Politis, 2015). The principles of vorticity control

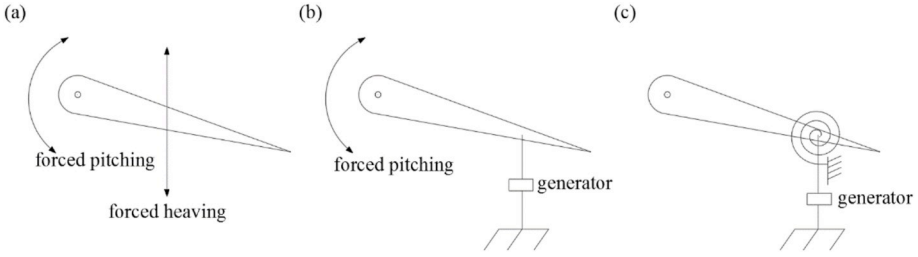

Fig. 6. Schematics of (a) full-active motion, (b) semi-active motion and (c) full-passive motion (Xiao and Zhu, 2014).

mechanism for the interaction between oncoming flow and fish body, fin and tail play a core role in understanding fish swimming and maneuvering.

3. Review on research methods

3.1. Experimental methods

The researches on flapping or oscillating foils done by a variety of scholars or teams from different countries adopt many kinds of experimental methods. A summary of past experimental studies of flapping foils or flat plates are presented in chronological order in Table 1. The range of each parameter and equipment used in experiments have more or less differences to obtain desired results for different objectives. Besides, flow visualization, velocity measurement, angle of attack profile, the cross-section and flexibility of a foil are also addressed in Table 1.

3.1.1. Environmental simulation

In experiments, the flow condition that a foil experiences is normally generated using a water or wind tunnel. The water tunnel has some common features, such as closed-circuit, free-surface, low speed, large-scale and low Reynolds number and their design principles do not bear too much difference. A re-circulating water channel used by Lua et al. (2016) and Dash et al. (2018) is shown in Fig. 7(a). The flapping mechanism mounted on the top of test-section can perform pitching with a resolution of 0.018° and heaving with a resolution of 0.005 mm. The greatest advantage of this system is that the vibration generated by linear motion (heaving) can be reduced to a minimum so that it has an unconsidered influence on the flow field (Lua et al., 2011). Most of water channels used before did not take this vibration into consideration. Generally, the water tunnels are horizontally placed with the flow going from one side to the other side. The exceptions are that Schnipper et al. (2009) and Andersen et al. (2017) innovatively used the vertically placed gravity-driven soap film tunnel to investigated the issues of oscillating foils, as shown in Fig. 7(c). The soap film tunnel not only has a good simulation of two-dimensional environment but is extremely advantageous to extend the area of wake downstream so that the far wake evolution can be visualized clearly. The development of flowing soap films has been reviewed by Schnipper et al. (2009). The characteristics of wind tunnel is generally similar to the water tunnel but the transmission medium is different. Sadeghi and Mani (2009, 2011 and 2015) investigated the effect of motion amplitude and mean angle of attack on the wake of an oscillating airfoil in a subsonic wind tunnel shown in Fig. 7(b). Because the wind speed of wind tunnel is high and the size of the airfoil is normally large, the corresponding Reynolds number has a relatively high order of magnitude compared with that in water tunnels. In ocean engineering field, a still water tank equipped with a towing carriage is normally used to simulate the relative motion between the fluid and obstacles. The study on propulsive efficiency of oscillating foils was conducted in the Ocean Engineering Testing Tank in MIT (Anderson et al., 1998; Read et al., 2003; Hover et al., 2004; Schouveiler et al., 2005) as shown in Fig. 7(d). The limitation of a still water tank is that the distance the foil can drive is short and the system vibration may have an effect on force measurement.

3.1.2. Flow visualization, velocity and force measurement

When we analyze the flow structure of the oscillating foil, the visualization and measurement of the flow are necessary. Some traditional methods including dye, hydrogen bubbles, soap film and smoke-wire flow visualization play an important role in qualitative observation of the wake structures. Dye and smoke-wire are mostly used for hydrodynamics and aerodynamics, respectively. It requires a good control of these medium so that the visualization can be up to the optimal. Fig. 8 shows a reverse Kármán vortex street generated by a pitching foil using dye flow visualization (Srigrarom and Vincent, 2008). Fig. 9 shows that smoke wire visualize the boundary-layers of the airfoil (Kim and Chang,

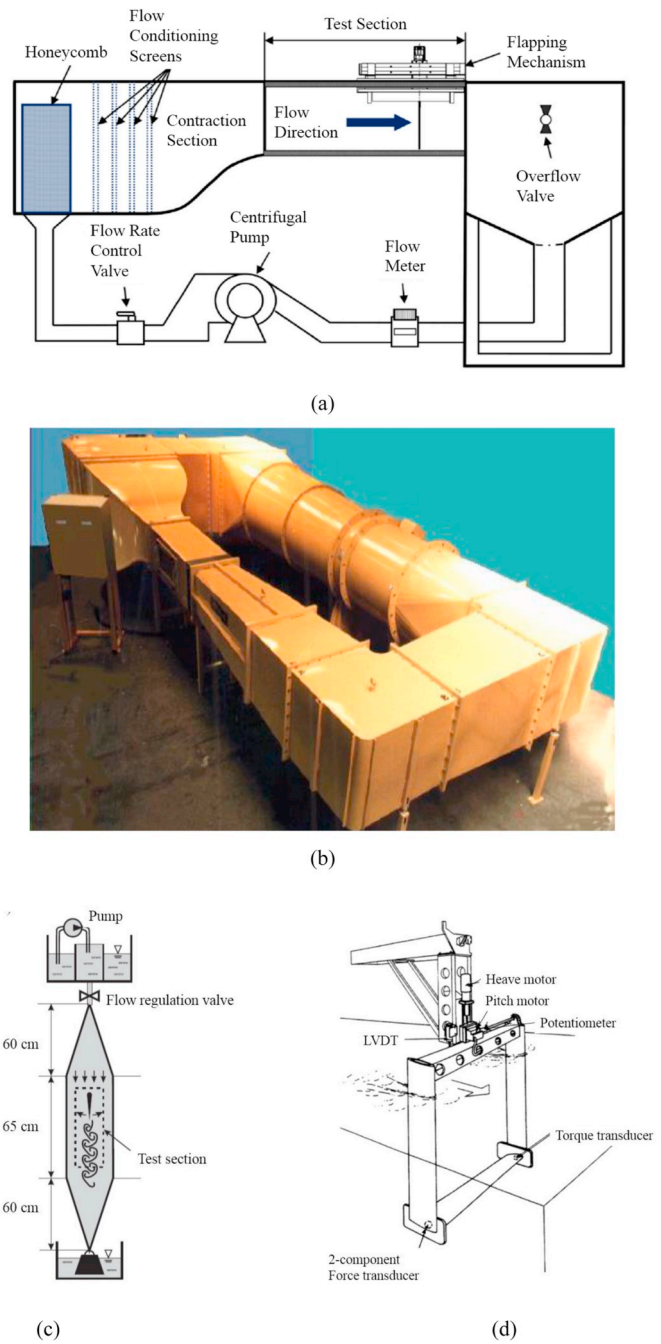

Fig. 7. Schematic of (a) a re-circulating water channel (Dash et al., 2018), (b) the soap film tunnel (Schnipper et al., 2009), (c) wind tunnel (Sadeghi et al., 2011) and (d) Ocean Engineering Testing Tank (Anderson et al., 1998).

2010). The flow velocity is measured mainly via hot wire/film anemometer (HWFA) in early days but it is still being used now (Chang and Yoon, 2002; Sadeghi and Mani, 2009; Sadeghi et al., 2011, 2015). The biggest disadvantage of this technique is the contact-type measurement, which interferes with the flow field greatly. Furthermore, laser Doppler velocimetry (LDV) achieves the non-contact 3D velocity measurement (Koochesfahani, 1989; Jones et al., 1998, 1999; Lai and Platzer, 1999; Kuo and Hsieh, 2001). However, both methods are only single-point measurement techniques and cannot obtain full-field and instantaneous measurement of the flow. At present, particle image velocimetry (PIV) shown in Fig. 10 is the most popular method used in experiments reviewed in Table 1. It can both display the physical form of flow field and provide quantitative information of instantaneous whole

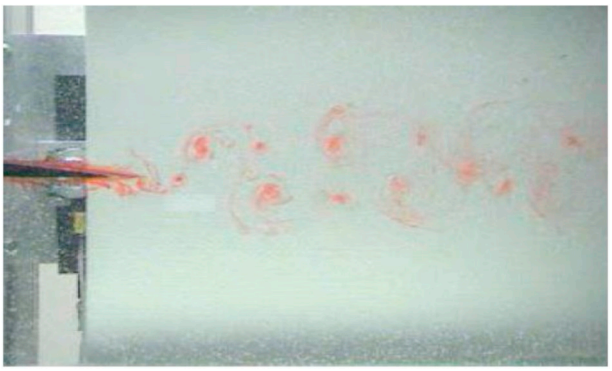

Fig. 8. Reverse Kármán Vortex Street via dye flow visualization (Srigrarom and Vincent, 2008).

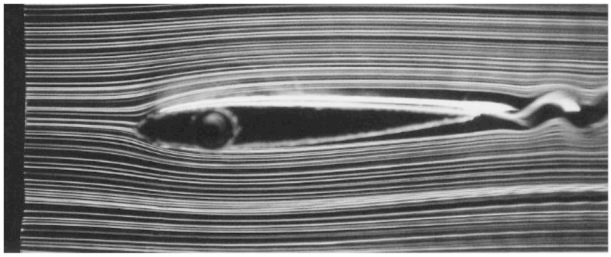

Fig. 9. Smoke-wire visualization of the boundary-layers of the airfoil (Kim and Chang, 2010).

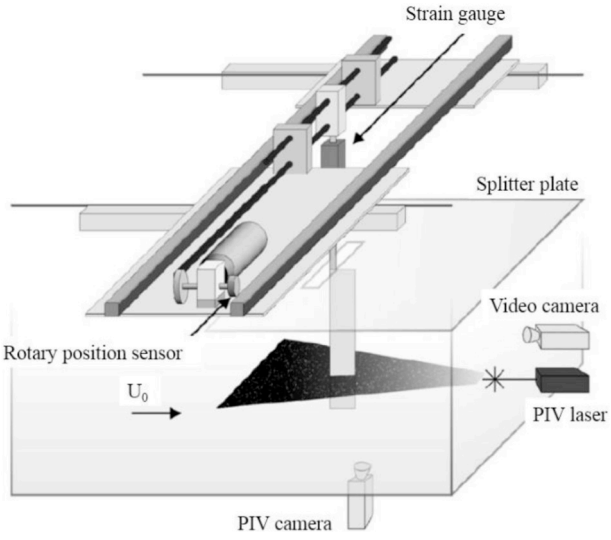

Fig. 10. Water tunnel experimental set-up for PIV measurements (Heathcote et al., 2008).

field flow, which makes the research of flow visualization leap from qualitative to quantitative. It also includes digital particle image velocimetry (DPIV) and stereoscopic particle image velocimetry (SPIV). Two more methods that need to be pointed out are the volumetric velocimetry (Calderon et al., 2014; Cleaver et al., 2016) and molecular tagging velocimetry (MTV), respectively. MTV is used to measure the vortical field of a foil oscillating at different reduced frequencies by Bohl and Koochesfahani (2009), which is considered as the molecular counterpart of PIV. The force measurement has been improved from using the strain gauge before to using high precision multi-directional force sensor now. Their measurement principle is not explained in detail here.

3.1.3. Experimental foil models

The physical properties of the research model are chosen based on the objective of the research and its geometric parameters have been introduced briefly in Section 2. NACA 4-digit foils, among which mainly NACA0012, are the most studied cross-sectional shape. In addition, flat plates which do not have the teardrop are also a research focus. Both of them have been reviewed in Table 1. More recently, a new concept of foil, as shown in Fig. 11(a), which combines a rigid NACA 4-digit foil in head location and a flat plate of variable flexibility in tail, receives a certain amount of attention from some researchers (Heathcote et al., 2004; Heathcote and Gursul, 2007; Monnier et al., 2015). Similarly, Kumar and Shin (2019) experimentally investigated the thrust estimation of a NACA0015 hydrofoil attached to an elastic plate with various lengths and breadths, whose construction is opposite to the previous foil, as shown in Fig. 11(b). Its wake vortex pattern and hydrodynamic performance due to flapping motion were discussed. For studies of a finite span flapping foil or flat plate, the three-dimensionality of the foil shape has a significant effect on aero/hydro-dynamic problems. Torres and Mueller (2004) studied the aerodynamics of four distinct geometries flapping wing planform (rectangular, Zimmerman, inverse Zimmerman and elliptical) with seven aspect ratios varying from 0.50 to 2.00 at various Reynolds numbers. Flow structures generated by variable planform (rectangular, semicircular, delta, circular, ring et al.) plates at different angles of attack (Freymuth et al., 1987; Taira and Colonius, 2009; Yilmaz and Rockwell, 2012) are also investigated. The flexibility of foil may affect the formation of leading edge vortex, trailing edge vortex and tip vortex and has been frequently considered in both spanwise (S. Heathcote et al., 2008; Cleaver et al., 2016) and chordwise (Prempraneerach et al., 2003; Bansmer et al., 2010; Alben et al., 2012; Barannyk et al., 2012; Dai et al., 2012; Marais et al., 2012; Dewey et al., 2013; Tian et al., 2013) directions. In addition, other properties including the chord length (Lai and Platzer, 1999; Alben et al., 2012), thickness (numerical method: Ashraf et al., 2011a; Yu et al., 2013; Sain et al., 2016; Wang et al., 2016c) and camber (Ashraf et al., 2011a; Chang et al., 2015) can also affect the dynamic performance of a foil. Thus, the geometry of the research model needs to be paid more attention so that the expected experimental results can be achieved.

3.1.4. Brief discussion of experimental parameters

In the reported experiments, the statistic characteristics for the foil are considered based on various parameters, such as Strouhal number (St), Reynolds number (Re), reduced frequency (k), aspect ratio (AR), dimensionless plunge/heave amplitude ($h = h_0/c$), phase angle between pitching and heaving motions (ϕ), pitch motion amplitude (θ_0) or nominal effective angle of attack (α_0), mean angle of attack (α_m), pivot location (X/c), and all of them have been described in detail in Section 2. The different definitions of the kinematic parameter Strouhal number have been presented. Due to the different physical meanings and definitions, the range of St is normally between 0.1 and 0.8 while the range of k is normally within 20 excepting that Lai and Platzer (1999) and Jones et al. (1998) studied wake structure of flapping foils at a high value of k up to 100. Similarly, environmental parameter Reynolds number also has many definition methods shown in Section 2. Re has a very wide range from 164 to 1.5×10^6 seen from Table 1 due to the different sizes of foils, incoming velocity and different definitions. Also, viscosity is another parameter that determines the Reynolds number Re. The fluid viscosity is determined by temperature and type of medium. For experiments, fluid viscosity is always taken as the value of water or air at 20 °C. In addition, Re is seldom altered by changing fluid viscosity for the researches on oscillating foil. The magnitude of Re determines the flow state which may be in laminar, transient or turbulent states. Different value of Re may result in completely distinct experimental results. Plunge/heave amplitude and pitch amplitude are inevitable basic parameters for the researches of flapping foils. There are three kinds of motion mode, including pure pitching, pure heaving and combined pitching and heaving as shown in Section 2. To some extent,

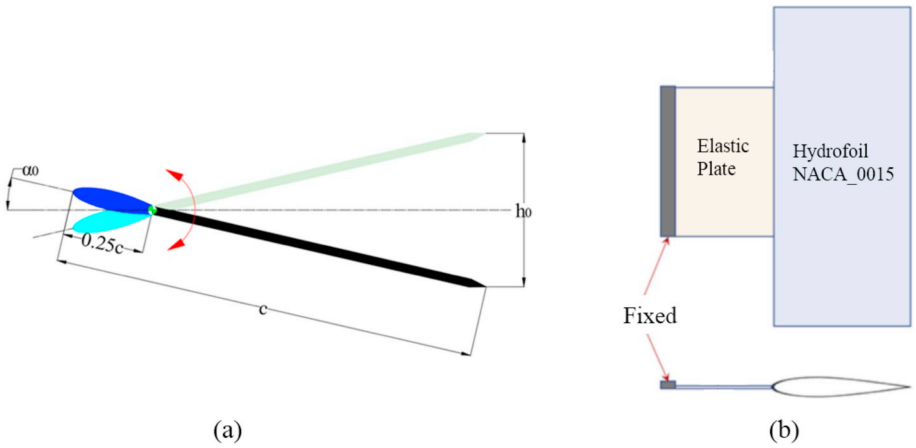

Fig. 11. Schematic of (a) a rigid NACA 4-digit foil in head and a flexible plate in tail (Monnier et al., 2015), (b) a NACA0015 hydrofoil attached to an elastic plate (Kumar and Shin, 2019).

flapping motion is equivalent to combined pitching and heaving (plunging) motion. Heave amplitude is generally no more than one chord length and pitch amplitude does not exceed 45° in Table 1 ϕ is generally fixed as 90° in the literature but the effect of phase angle on performance of the foil is also investigated (Anderson et al., 1998; Read et al., 2003; von Ellenrieder et al., 2002, 2003). The range of ϕ presented is from 30° to 120°. Similarly, α_m is always fixed as 0° but the effect of mean angle of attack on foils is also discussed (Ohmi et al., 1990, 1991; Jones et al., 1999; Lee et al., 2000; Schouveiler et al., 2005; Srigrarom and Vincent, 2008; Sadeghi and Mani, 2009, 2011; Cleaver et al., 2012; Hu et al., 2013). The range of α_m is from 0° to 45° but most of them focus on small angle of attack. Moreover, variable pivot location (Granlund et al., 2013; Tian et al., 2016; Mackowski and Williamson, 2017) and non-sinusoidal motion (Hover et al., 2004; Fenercioglu et al., 2015; Karakas and Fenercioglu, 2016; Van Buren et al., 2017; Dash et al., 2018) also influence the flow structures and hydrodynamic forces of the foil. The specific effect of Reynolds number, reduced frequency, three-dimensional effect (AR) and motion amplitude will be discussed in Section 4.

3.2. Numerical works

The statistics whose classification criteria is almost the same as experimental works are also done for numerical works as shown in Table 2.

3.2.1. Numerical approach

Nowadays, Computational Fluid Dynamics (CFD) CFD is the main method used for researches on the dynamics of flapping foils or plates but the method of Non-CFD develops early and is still used today. Panel method is one of the widely used methods in early days (Jones and Platzer, 1997; Jones et al., 1999). Guglielmini and Blondeaux (2004) solved governing equations of an oscillating foil using a stream-function vorticity formulation for a two-dimensional problem. This method is also adopted recently (Zhu et al., 2009; Zhu, 2011, 2012). Particularly, Andersen et al. (2017) performed the numerical simulations of wake structure of a flapping foil in 2D flow using the particle vortex method (PVM). This method has been described and validated by Walther and Larsen (1997), Larsen and Walther (1997), Rasmussen et al. (2010) and Hejlesen et al. (2015). However, with the maturity of computer technology, CFD has become the main method to investigate fluid problems. The implementation of CFD frequently depends on some commercial or open-source codes, such as Fluent, CFX, StarCCM+ and OpenFOAM, most of which are based on finite volume method (FVM) and a few of which are based on finite element method (FEM) and finite difference method (FDM). Yu et al. (2017) investigated the effect of kinematic parameters on the propulsion performance of an oscillating foil at Re from 10^3 to 1.6×10^6 using FVM with the Spalart-Allmaras (S-A) turbulence model and they concluded three different combinations of kinematic parameters for optimal propulsion efficiency. Lua et al. (2016) use Fluent based on FVM to study the thrust performance of a flapping 2D elliptic airfoil in forward flight numerically and their results show that high rotation rate of the foil causes an adverse suction effect which can suppress the thrust of the foil. Boiron et al. (2012) used the FEM to solve the flow around the foil and they compared the hydrodynamics of a flapping foil through experimental and numerical methods. Meanwhile, spectral method (SM) and Lattice Boltzmann Method (LBM) are non-grid-based approaches. Yu et al. (2012, 2013) adopted an unsteady compressible Navier-Stokes (N–S) solver using high-order spectral difference (SD) method to investigate the wake structure and the effects of foil thickness and kinematics on flapping foil propulsion. Medjroubi et al. (2011, 2012) simulated the 2D unsteady flow around a heaving NACA0012 airfoil using the spectral element method (SEM) and well reproduced the wake flow behind the heaving foil. Wu et al. (2014, 2015a,b,c) used the immersed boundary-lattice Boltzmann method (IB-LBM) to simulate the flow over the foil so that the energy extraction performance can be obtained. The numerical results obtained from direct CFD simulations make significant contributions to improving the thrust and propulsive efficiency of a flapping foil and provides a theoretical basis for follow-up researches. Besides the methods mentioned above, immersed boundary fractional-step method (IBFS) (Choi et al., 2015), a high-fidelity implicit large-eddy simulation (ILES) (Visbal, 2009; 2013) etc. are also used in numerical simulations. Moving mesh method is an essential issue for the numerical study of an oscillating foil. There are many moving mesh methods. Elastic scaling method and mesh reconstruction method are commonly used to simulate pitching and heaving motions.

3.2.2. Turbulence models

There are three kinds of methods to simulate the turbulence flow of flapping foils, namely Direct Numerical Simulation (DNS), Large Eddy Simulation (LES) and Reynolds-Averaged Navier-Stokes (RANS). Base on the literature review, RANS is the early method used to solve the issues of turbulence. It has been used for a wide range of Re for studies on flapping foils. However, RANS cannot obtain satisfactory results for the turbulent flow structures. DNS can accurately get all information of turbulence and do not consider the closeness of the equations, but it is limited to low Re and simple boundary problems due to its high demand on computational resources. Actually, LES is superior to RANS in terms of model construction and is computationally more efficient than DNS (although its computational cost is still high), but its development is not yet mature and is only for simple shear and tube flow. Turbulence

models are used to close the governing equation. Several models, such as single-equation Spalart-Allmaras (S-A) turbulence model, two-equations shear-stress transport (SST) turbulence model, k-ω two-equations SST turbulence model and zero-equation Baldwin–Lomax (B-L) algebraic turbulence model, are listed in Table 2. Zhu et al. (2015) used the S-A turbulence model to close RANS and found that the energy harvesting efficiency of a new adaptive deformation oscillating foil they proposed can be 16.1% higher than the conventional one without deformation. Kinsey and Dumas (2012) carried out a numerical research based on 2D unsteady RANS simulations using S-A model and analyzed the different tandem configuration for two oscillating foils within a hydrokinetic turbine to maximize the energy harvesting efficiency. Liu et al. (2013) utilized a bio-inspired flexible flapping foil to discuss the energy harvesting performance using k-ω turbulence model for unsteady RANS closure. They concluded that the flexible structure or the parallel configuration of the foil all can enhance energy efficiency. Münch et al. (2010) proposed a method using SST k-ω and k-ε turbulence model that can predict fluid-structure coupling for a rigid hydrofoil with forced and free pitching motions. Kang et al. (2009) studied the effects of chord length based Reynolds number on the dynamics of the oscillating SD7003 airfoil by solving 2D RANS based on SST model, which is compared with experimental results. Lu et al. (2013a,b) used SST k-ω model for simulations to investigate the effects of asymmetric sinusoidal motion on pitching airfoil aerodynamics. Tuncer and Kaya, (2005, 2007) adopted the B-L algebraic turbulence model to optimize the thrust and propulsion efficiency of flapping foils through different methods. In addition, there are other turbulence models, such as Zero-equation Cebeci-Smith (C–S), single-equation Baldwin-Barth (B–B) and Reynolds stress model (RSM), but most of them are not suitable for the issues related to the oscillating foil.

3.2.3. Brief discussion of numerical parameters

Columns 6 to 17 in Table 2 are based on the same classification of the physical properties and kinematic parameters of the flapping foil or plate as in the experimental work. The specific content also has more or less similarity. NACA series are frequently chosen to be the research object, of which mainly NACA0012. The stiffness of the foil are mostly rigid although the effect of chordwise (Miao and Ho, 2006; Shin et al., 2009; Eldredge et al., 2010; Tay and Lim, 2010; Ysasi et al., 2011; Zhu et al., 2014a,b; Liu et al., 2016; Olivier and Dumas, 2016a,b; Jeanmonod and Olivier, 2017) and spanwise (Zhu, 2007; Kang et al., 2011) flexibility of the foil is also studied in numerical approaches. Noteworthily, the range of Re is a little different from that in the experiments in Table 1. The smallest Reynolds number is 100 and the highest up to 9.38×10^6. The discussions on three-dimensional effect are always unavoidable. The effect of AR has been studied (Dong et al., 2006; Shao et al., 2010; Li and Lu, 2012; Harbig et al., 2013; Deng et al., 2015), the range of which summarized in Table 2 is from 0.2 to 8. The range of pitching amplitude θ_0 (or maximum angle of attack α_0) considered in numerical simulations is wider than that in the experiments. Similar with the experimental studies, the effect of phase angle ϕ (Jones and Platzer, 1997; Ramamurti and Sandberg, 2001; Pedro et al., 2003; Tuncer and Kaya, 2005; Eldredge et al., 2010; Platzer et al., 2010; Sarkar and Singasani, 2009; Xiao and Liao, 2010; Ashraf et al., 2011b), mean angle of attack α_m (Visbal and Shang, 1989; Ohmi et al., 1991; Jones et al., 1999; Visbal, 2009; Sarkar and Singasani, 2009; Medjroubi et al., 2011; Liu et al., 2013; Martín-Alcántara et al., 2015), non-sinusoidal motion (Kaya and Tuncer, 2007; Xiao and Liao, 2010; Xiao et al., 2012; Esfahani et al., 2013; Lu et al., 2013a,b; Young and Lai, 2014; Lu et al., 2014; Teng et al., 2016) and pivot location (Zhu et al., 2009; Eldredge et al., 2010; Zhu, 2011, 2012; Wang et al., 2017a) have also been investigated numerically. Particularly, the effect of the relative position between an upstream bluff body and a heaving and pitching hydrofoil on energy harvesting performance has been investigated by Lahooti and Kim (2019). They found that the presence of the upstream body can change flow structure around the hydrofoil, thus improve the efficiency significantly.

4. Review on the law of several significant parameters

As aforementioned, the dynamic characteristics of the flapping foil are dependent on various factors which have been introduced in Section 2.2. In this section, the related conclusions of four major parameters, including Reynolds number Re, reduced frequency k, pitch or heave amplitude and three-dimensional effect, are reviewed from three aspects: flow structures, hydrodynamic coefficient and energy harvesting efficiency.

4.1. Reynolds number

Reynolds number is the fundamental parameter determining the flow status and has been considered in a wide range from 10^2 to 10^7 for the flapping foil. It is a significant conclusion that the variation of Reynolds number has no apparent effect on the formation of the periodic vortex and establishment of the subsequent wake behind an oscillating foil in the range of $1500 < Re < 10^4$ (Ohmi et al., 1990). Ashraf et al. (2009) and Medjroubi et al. (2011) performed simulations on a pure plunging foil, and found that flow structure was almost independent of Reynolds number for $\mathrm{Re} = 200\text{-}2 \times 10^5$ and $Re = 800$–8000, respectively. Baik and Bernal (2012) carried out experiments on a pitching and plunging foil came to the same results with Ashraf et al. and Medjroubi et al. for Re between 10^4 and 6×10^4. Fenercioglu and Cetiner (2012) also made a similar conclusion that five flow structure categories generated by a combined pitching and plunging foil are independent of increasing Reynolds number from 825 to 1.37×10^4 and even the production of thrust is independent on the Reynolds number for $Re < 1.5 \times 10^4$. Leading edge vortex (LEV) and trailing edge vortex (TEV) are frequently seen from wake structures behind a flapping foil. Both of them are sensitive to the variation of Reynolds number. Lu et al. (2013a,b) and Ol et al. (2008) investigated the trapezoidal-pitch SD7003 airfoil at different Re and they clearly observed that the attenuation of the LEV decreased when Re increased from 300 to 1200, resulting in a stronger interaction between the LEV and TEV. Kang et al. (2009) concluded that leading edge vortex formed at lower Re ($Re = 10^4$) and more attached flow is observed at higher Re ($Re = 3 \times 10^4$, 6×10^4) for combined pitching and plunging case. However, for pure plunging case, the leading edge vortex occurred at all investigated Re, which became stronger with increasing Re. Amiralaei et al. (2010) observed the vortical patterns around a NACA0012 pitching airfoil, as shown in Fig. 12. The TEV and the lower surface vortex became larger and stronger with Re increasing from 555 to 1000. Further increasing to 2000, lower surface vortex started to separate but TEV had not yet. In contrast to $Re = 2000$, TEV was separated and downstream convected but the lower and upper surface vortices attached on the foil at $Re = 5000$. Varied Reynolds number is the root cause to the existence of this phenomenon of unsteady boundary layer separation and reattachment. The increase of Reynolds number gives rise to the promotion (delay) of the reattachment and unsteady laminar separation during the upstroke (downstroke) of the pitching foil, which is obtained by Kim and Chang (2010). Generally, the wake behind a pitching or heaving foil is symmetric about the middle position of the foil periodic motion. However, when a foil pitches or plunges at relatively high frequency and large amplitude, symmetry-breaking occurs in the vortical wake, leading to a deflection angle which is related to Reynolds number. Liang et al. (2011) were the first to find that the deflection angle increases with Reynolds number increasing for a fast plunging airfoil as shown in Fig. 13. Subsequently, Zheng and Wei (2012) conducted further researches on mechanism of this phenomenon. For a finite foil, the effect of Reynolds number on its three-dimensional vortex structure was also investigated numerically and experimentally by Visbal et al. (2013). They found that spanwise fine-scale transitional features from no evidence to becoming more obvious when Reynolds number increases from 10^3 to 5×10^3. Ol (2007) proved that the

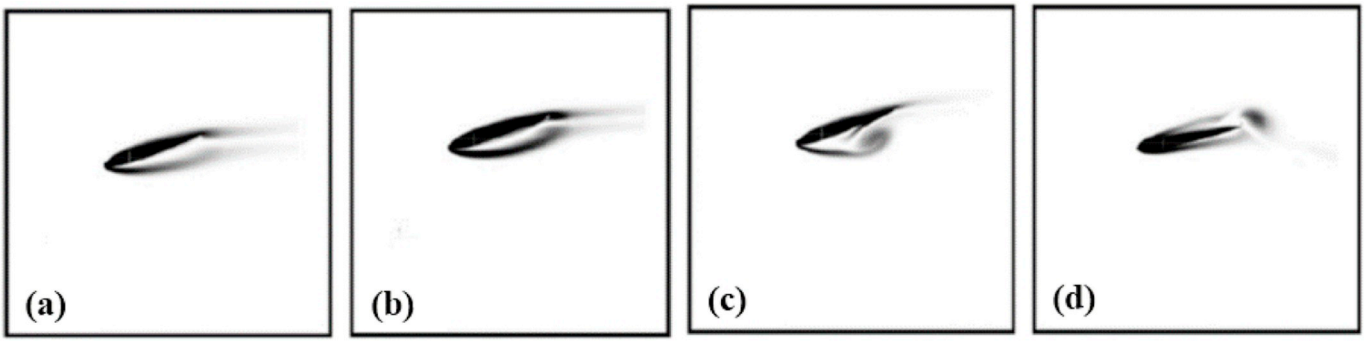

Fig. 12. Vortical patterns around a NACA0012 pitching airfoil at (a) Re = 555, (b) Re = 1000, (c) Re = 2000 and (d) Re = 5000 (Amiralaei et al., 2010).

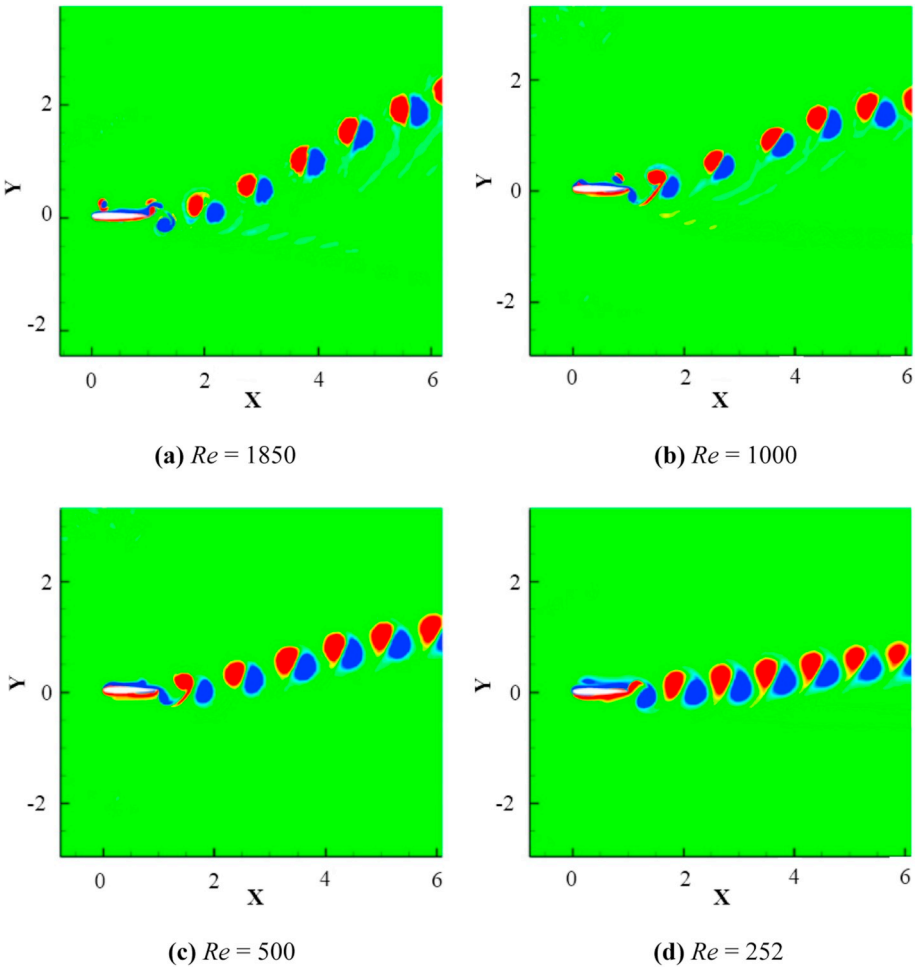

Fig. 13. Vorticity around a fast plunging airfoil at different Reynolds numbers (Liang et al., 2011).

strength of spanwise flow increases with increasing *Re* from 10^4 to 6×10^4.

The influence of Reynolds number on hydrodynamic/aerodynamic coefficient of a pitching, plunging or oscillating foil including the coefficient of lift, thrust, drag and power is also discussed here. Miao and Ho (2006) simulated the power coefficient of a flapping flexible airfoil at different Reynolds number (10^2, 10^3, 10^4) which is found to have no effect on both thrust and input power coefficient, as shown in Fig. 14. The same results were obtained for a spanwise flexible flapping wing and a rigid pitching foil by Heathcote et al. (2008) and Das et al. (2016), respectively. Similarly, Reynolds number hardly affects force generation for a flapping foil. Lua et al. (2010) studied the Reynolds number from 7800 to 1.17×10^4 and found Reynolds number has a very small effect on the force generation. Medjroubi et al. (2011), Baik et al. (2012) and Baik and Bernal (2012) made similar conclusions that the influence of Reynolds number on aerodynamic force generation is weak. In addition, Heathcote et al. (2008) provided a result that the thrust coefficient is a very weak function of Reynolds number and Lua et al. (2008) obtained that the mean drag coefficient has nothing to do with the Reynolds number. However, the law of Reynolds number is not true for all cases. Ashraf et al. (2009) investigated the NACA0015 plunging airfoil at $Re = 2 \times 10^5$, which generates 40% more thrust than that at $Re = 2 \times 10^4$. Time-averaged thrust coefficient increases with increasing Reynolds number ($Re = 72$, 144 and 360) based on the flapping airfoil thickness in

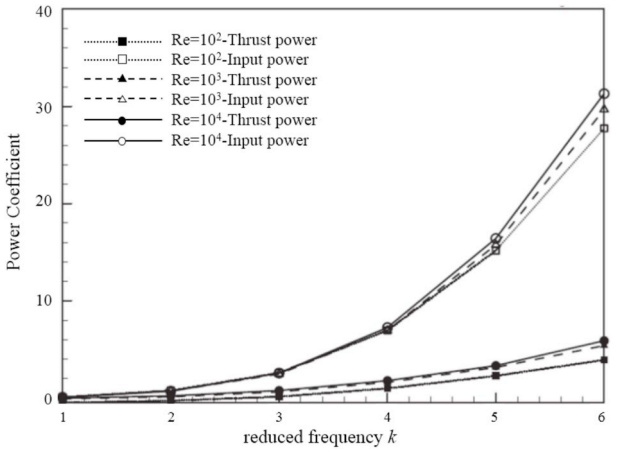

Fig. 14. Thrust and input power coefficient varied with reduced frequency at Re = 10^2, 10^3,10^4 (Miao and Ho, 2006).

the simulation performed by Yu et al. (2013). Das et al. (2016) also obtained the same result for a pitching foil at different Re from 10 to 2000. Furthermore, Visbal (2009) and Liang et al. (2011) found that the drag coefficient decreases evidently as the Reynolds number increases for a pure plunging foil and a plunging and pitching foil, respectively.

Reynolds number has a relatively uniform influence on propulsive or energy harvesting efficiency. Generally, the efficiency increases with Reynolds number. Miao and Ho (2006) observed that the propulsive efficiency increases with increasing Reynolds number at lower reduced frequency for a chordwise flexible flapping airfoil and Heathcote et al. (2008) also concluded that the efficiency increases slightly with Reynolds number for a spanwise flexible flapping foil. In addition, Ashraf et al. (2009) investigated the Reynolds number on a pure plunging NACA0015 airfoil propulsive at reduced frequency $k = 2$, non-dimensional plunge amplitude $h = 0.5$ and results revealed that propulsive efficiency increases with Re increasing from 20 to 2×10^5 as shown in Fig. 15(a). Fig. 15(b) shows that the propulsion efficiency rises significantly as *Re* increase; after that, only slight change can be observed (Lin et al., 2019). Optimal energy harvesting efficiency is found to be enhanced by increasing Reynolds number by Zhu (2011).

4.2. Reduced frequency

Reduced frequency is a type of non-dimensionalized expression of frequency, defined as $k = 2\pi fc/2U_\infty$, identified as the major parameter controlling flow development. The flow structure changes apparently as the reduced frequency varies. Bohl and Koochesfahani (2009) presented an experiment on vortical structure in the wake of a pitching NACA0012 airfoil using molecular tagging velocimetry (MTV), observing that a Kármán street with alternating sign vortices (clockwise vortices at the top of the centerline, counter clockwise at the bottom of the centerline) at $k = 5.2$, a neutral wake (alternating sign vortices nearly aligned along the wake) at $k = 5.7$ and a reverse or inverted Kármán street with alternating sign vortices (counter clockwise vortices at the top of the centerline, clockwise at the bottom of the centerline) at $k = 11.5$. The similar phenomenon was revealed by Medjroubi et al. (2012) for a heaving NACA0012 airfoil using the spectral/hp element method at $k = 0$, $k = 4.52$ and $k = 7.85$, respectively. Recently, Moubogha et al. (2017) obtained similar results for a pitching plate at $k = 1.5$–5 via the comparison of experimental and numerical method, as shown in Fig. 16. All of aforementioned results are well consistent with the previous ones observed in Koochesfahani (1989). Some detailed changes of vortices (leading and trailing edge vortices) around a foil with varied reduced frequency are further investigated. Ol (2007) used dye visualization to display the vortex shedding behind the trailing edge of a pure plunging airfoil. He observed that the wake adjacent to trailing edge varies from a planar and uniform flow into a starting vortex with increasing reduced frequency and larger reduced frequency leads to greater persistence of the starting vortex. Baik et al. (2012) noticed that increasing reduced frequency causes slower LEV and TEV growth rate through PIV measurements for a flapping airfoil. Moreover, Panah and Buchholz (2014) observed four categories of wake patterns which are mainly dependent on reduced frequency within the range of $0.39 < k < 4.7$ for a 2D plunging plate, (i) LEV merges with like-signed TEV, (ii) LEV interacts with the following stronger opposite-signed TEV, (iii) LEV arrived at trailing edge one full period latter than the opposite-signed TEV generation and (iv) LEV remains on the surface of airfoil for more than three strokes. The strength of LEV is reduced when it sheds into wake with increasing reduced frequency *k* (see Fig. 17).

The effect of reduced frequency on hydro/aerodynamic coefficient studied by many researchers has no qualitative difference. Generally, the mean thrust coefficient tends to increase with reduced frequency. Garrick (1936), Koochesfahani (1989) and Ramamurti and Sandberg (2001) firstly used the theoretical, experimental and numerical methods to reach this result, respectively. Mackowski and Williamson (2015) reviewed some relatively early studies on mean thrust of a pure pitching foil from theory (Garrick, 1936; Jones and Platzer, 1997; Ramamurti and Sandberg, 2001), simulation (Ramamurti and Sandberg, 2001; Young and Lai, 2004) and experiment (Koochesfahani, 1989; Bohl and Koochesfahani, 2009), compared with their own direct force measurements of thrust, shown in Fig. 13. As shown in Fig. 13, all of them has the same increasing trend with reduced frequency although their results exist a quantitative difference due to the distinct conditions. However,

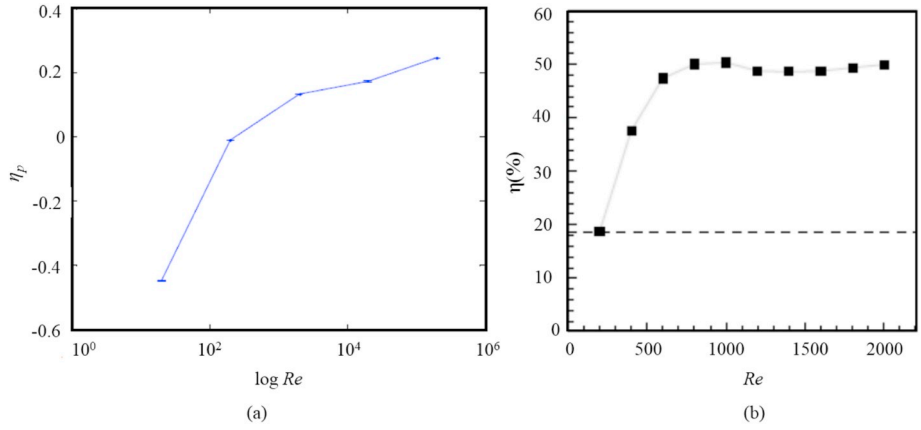

Fig. 15. Effect of *Re* variation on efficiency of (a) a plunging NACA0015 airfoil at $k = 2$, $h = 0.5$. (Ashraf et al., 2009), (b) a combined oscillating NACA0012 foil in stationary fluid (Lin et al., 2019).

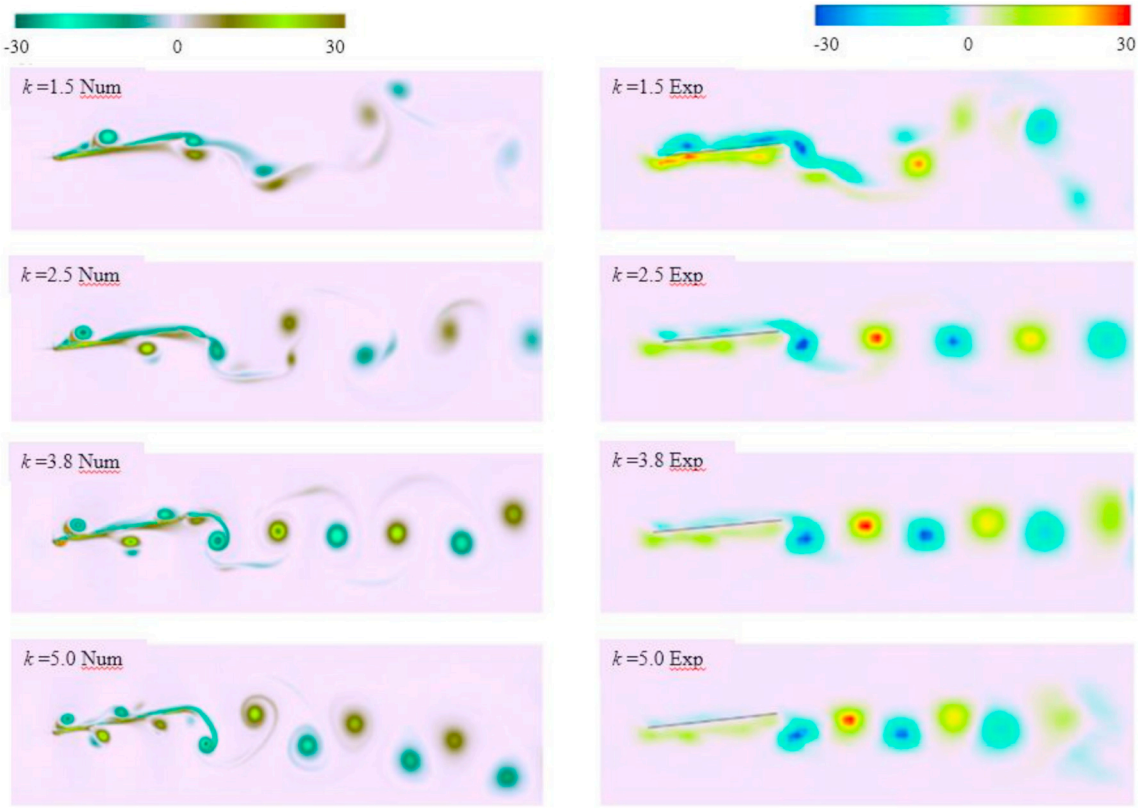

Fig. 16. Numerical (left column) and experimental (right column) flow structures around a pitching plate for $k = 1.5$, 2.5, 3.8 and 5, for an angle of attack of $-8°$. (Moubogha et al., 2017).

the change of other parameters appears having very limited influences on the trend of mean thrust coefficient. For instance, the experiments or simulations for a plunging airfoil (Ashraf et al., 2012; Elarbi, 2013), a non-sinusoidal pitching airfoil (Lu et al., 2013a,b; Zaman et al., 2014), a flexible pitching panel (Dewey et al., 2013) and a combined pitching and plunging airfoil (Esfahani et al., 2015) all show that the increase of reduced frequency causes a noticeable increase in mean thrust coefficient and thus suggests that the motion modes, motion profile and flexibility of a foil do not alter this conclusion. It should be pointed out that there is a maximum thrust coefficient after which it starts to decrease slightly with further increasing reduced frequency k for a flexible pitching plates obtained by Dewey et al. (2013) and this change is also clearly observed within the range of $1.82 \lesssim k \lesssim 10.92$ for a pitching airfoil by Ashraf et al. (2015). The power coefficient showed similar trends as those of mean thrust coefficient. For a flexible pitching plate, the power coefficient increases to a maximum and then levels off (Dewey et al., 2013).

The reduced frequency is a key parameter in analysis of propulsion and power extraction by flapping foil. The reduced frequency determines the magnitude of energy that the flapping foil can extract from free stream. The variation trend of propulsive efficiency of a flapping foil propeller with reduced frequency is similar to a reverse parabola, displaying that propulsive efficiency increases monotonically with reduced frequency k at first and then it decreases gradually with further increasing k when other parameters are fixed (Ashraf et al., 2012; Lu et al., 2013a,b; Elarbi, 2013; Dewey et al., 2013; Esfahani et al., 2015). The magnitude of efficiency is not fixed owing to a variety of other parameter combinations, such as pitching or heaving amplitude, the flexibility of the foil and phase angle between pitching and heaving. However, there is a truth that the maximum propulsive efficiency always occur at relatively low k. Moreover, at the same k, the flexible foil can further enhance the efficiency, even resulting a doubled efficiency. The qualitative trend of power extraction efficiency of a flapping foil energy harvester with forced pitching and heaving motions almost has no difference in propulsive efficiency (Liu et al., 2013; Xie et al., 2014; Karbasian et al., 2015; Lu et al., 2015; Wu et al., 2016; Xu and Sun, 2016) as shown in Fig. 18. Similarly, the global optimal energy extraction efficiency also appears at low k within the range between 0.1 and 0.15 which has been summarized specifically by Xiao and Zhu (2014) and explained physically by Zhu (2011). For the semi-active flapping foil, the energy extraction efficiency is different from that of the fully-active flapping foil. Wu et al. (2014, 2015a,c) simulated the power extraction of a semi-active flapping foil with the auxiliary foil, the flexible tail and different spring constant respectively, all of which come to the same conclusion that energy extraction efficiency monotonically decreases with increasing reduced frequency, as shown in Fig. 19.

4.3. Pitching or heaving amplitude

The influences of pitching or heaving amplitude on the flow structures are globally similar with that of the reduced frequency. This can be sketched that when flapping frequency and other parameters are fixed, as the flapping amplitude increases, the flow structure initially transits from Kármán street to aligned vortices, and then becomes reverse Kármán street, and finally become deflected reverse Kármán street with symmetry breaking. Essentially, the global flow structure of a single general flapping foil mainly depends on frequency and amplitude. Godoy-Diana et al. (2008) uses the experimental method to investigate the transitions in the wake of a pitching foil with different amplitude and frequency combination and obtained aforementioned transition process of the flow structure. He et al. (2012) also proved this process via a numerical method. Schnipper et al. (2009) and Andersen et al. (2017) compared numerical and experimental investigations for the flapping foil and measured the phase diagram in the (St_A, A_D) space as shown in Fig. 20, where St_A and A_D are another form of non-dimensional frequency and amplitude, respectively. In addition, the distribution of flow

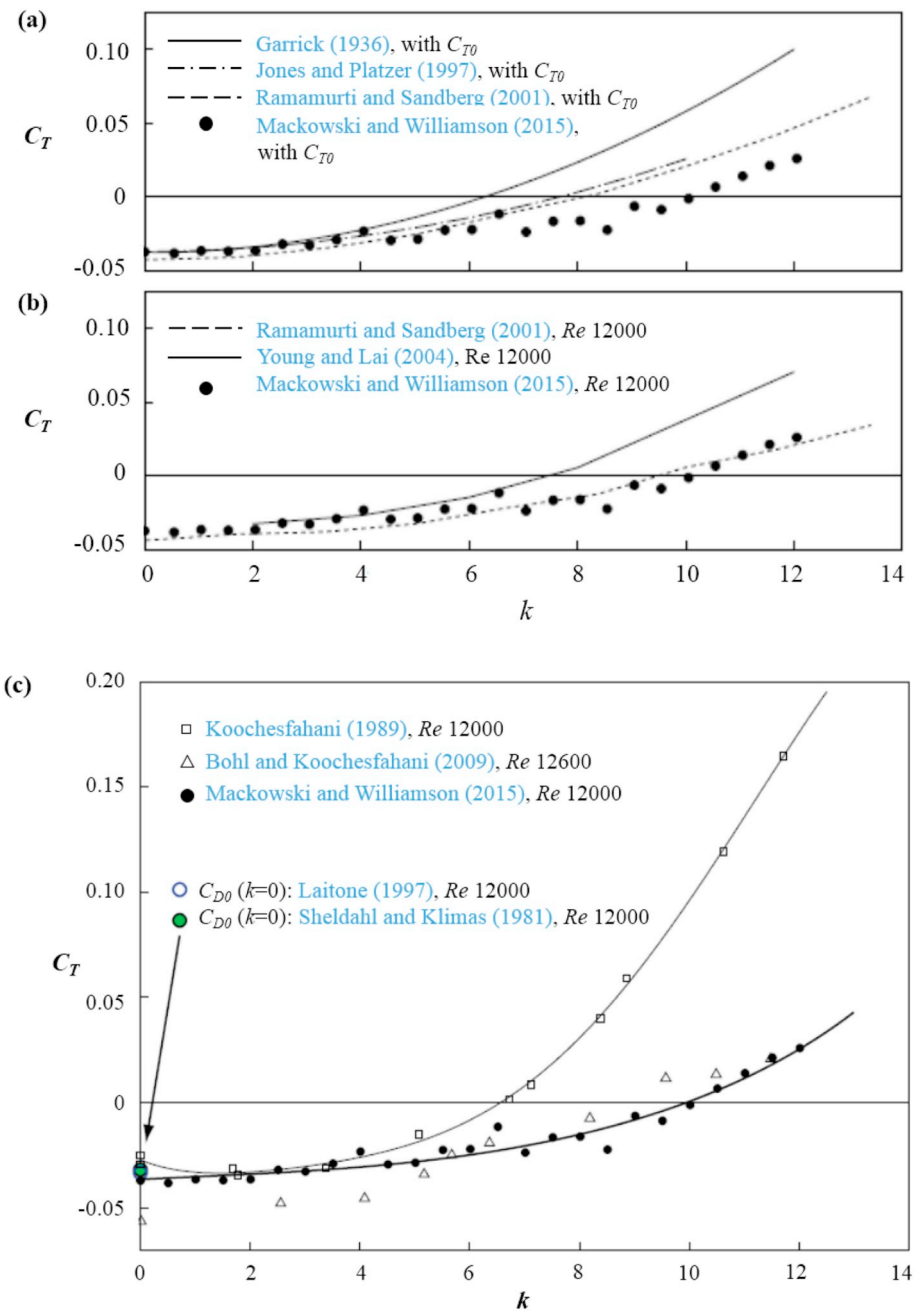

Fig. 17. (a) Theoretical, (b) simulation and (c) experimental values of thrust coefficient for a NACA 0012 pitching airfoil. (Mackowski and Williamson, 2015).

patterns of a pitching foil and a heaving foil is almost same qualitatively. Leading edge vortex is also affected by the variation of amplitude. The convection of leading edge vortex along the chord becomes faster and the strength of the vorticity increases with increasing plunging amplitude (Panah and Buchholz, 2012). Besides, the leading edge vortex becomes severer and the scale becomes larger with pitching amplitude increasing from 5° to 40° as investigated by Xie et al. (2014).

The pitching or heaving plunging amplitude are also the crucial parameters affecting the hydrodynamic coefficients. Here we mainly focus on the thrust, power coefficient and propulsive efficiency. When other parameters are fixed, the power imparted to oscillating a foil increases with pitching or heaving amplitude, resulting a monotonic increase of the power coefficient. The increase of pitching and heaving amplitudes cause to the thrust coefficient increasing to a maximum, and then it begins to decrease because the thrust enhancement becomes negative for large amplitude cases. The propulsive efficiency represents the ratio of the thrust power to the power input to the foil. Consequently, the propulsive efficiency presents two different variation trends. If the enhancement of thrust coefficient is more than that of power coefficient at low amplitudes, the trend of propulsive efficiency is similar to that of thrust coefficient. Otherwise, the propulsive efficiency decreases monotonically with increasing amplitudes. However, these general conclusions from the previous studies (Amiralaei et al., 2010; Lu et al., 2013a,b; Zaman et al., 2014; Das et al., 2016; Yu et al., 2017) are not always true for thrust coefficient, power coefficient and propulsive efficiency. For instance, small values of pitching amplitude ($\theta_0 < 10°$) has small effect on propulsive efficiency (Mackowski and Williamson, 2015). Thrust coefficient could continuously increase with heaving amplitude within a relatively large range ($h_0/c < 1.5$) (Ashraf et al., 2012). Power coefficient also can increase firstly and then decrease gradually with increasing pitching amplitude (Srigrarom and Vincent, 2008).

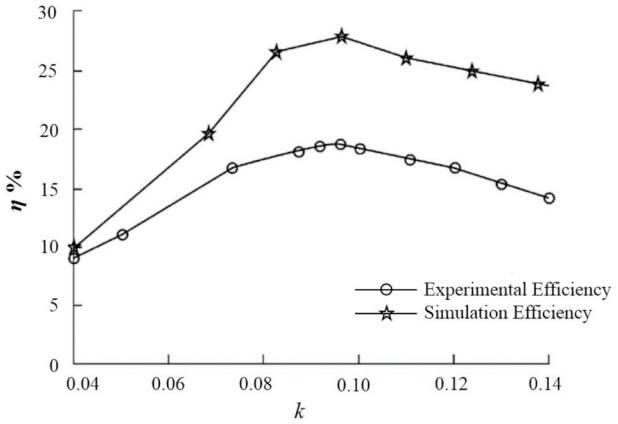

Fig. 18. Energy extraction efficiency as a function of reduced frequency (Xu and Sun, 2016).

The influence of pitching and heaving amplitudes on power extraction performance is very complex and there is no universal law. Therefore, here we can only give some general rules based on the relevant studies. If we want to reach the power extraction state, a condition needs to be satisfied that the angle of attack induced by heaving motion must be smaller than the pitching angle, which has been investigated by Jones and Platzer (1997). Generally, no matter for forced pitching and heaving or forced pitching and induced heaving motions, the energy extraction efficiency contribution from pitching motion is quite limited and much smaller than that from heaving motion. For forced pitching and heaving motion, when other parameters are fixed, the energy extraction efficiency increases with heaving amplitude at low range ($h_0/c < 1.0$). This law has been summarized by Xiao and Zhu (2014). For forced pitching and induced heaving motion, when other parameters are fixed, the energy extraction efficiency firstly increases monotonically with pitching amplitude and then reaches a peak after which it decreases with further increasing pitching amplitude. Particularly, if reduced frequency k does not exceed 0.5, the pitching amplitude of the maximum efficiency should generally be located between 60° and 80° as shown in Fig. 21(a). Besides, the optimal pitching amplitude decreases with gradually increasing k as shown in Fig. 21(b). These rules can also be applied to forced pitching and heaving motions.

4.4. Three-dimensional effect

Since the aero/hydro-foil in nature is always finite in spanwise length, the results concluded under the assumption of infinite spanwise length or two dimensions are no longer applicable. The hydrodynamic characteristics of an oscillating foil are significantly affected by the shape at its ends. von Ellenrieder et al. (2003) and Parker et al. (2007) (Soria's team) discussed the effect of amplitude and frequency of the oscillating foils with a finite aspect ratio on the structure of 3D vortices at low Reynolds number ($Re = 164$) through dye visualization and PIV. They concluded that due to the tip vortices of the foil, the global vortices structure takes a great change, which is completely different from that generated by the 2D foil, as shown in Fig. 22. Jardin et al. (2012) studied the three-dimensional effect of flow around a NACA0012 airfoil with combined pitching and heaving motion and it revealed that the interaction between leading edge vortices and spanwise vortices were very strong. Green et al. (2011) (Smits' team) used PIV to analyze the 3D flow structure of the trapezoid with pure pitching motion. This trapezoid foil was inspired by fish caudal fin. The experiment suggested that inclined diversion edge can generate more complex tip vortices. Actually, the generation of spanwise vortices and tip vortices are the main reason for making the flow structure of the 3D foil more complex compared with the 2D foil.

Buchholz and Smits (2008) found that thrust coefficient of the foil

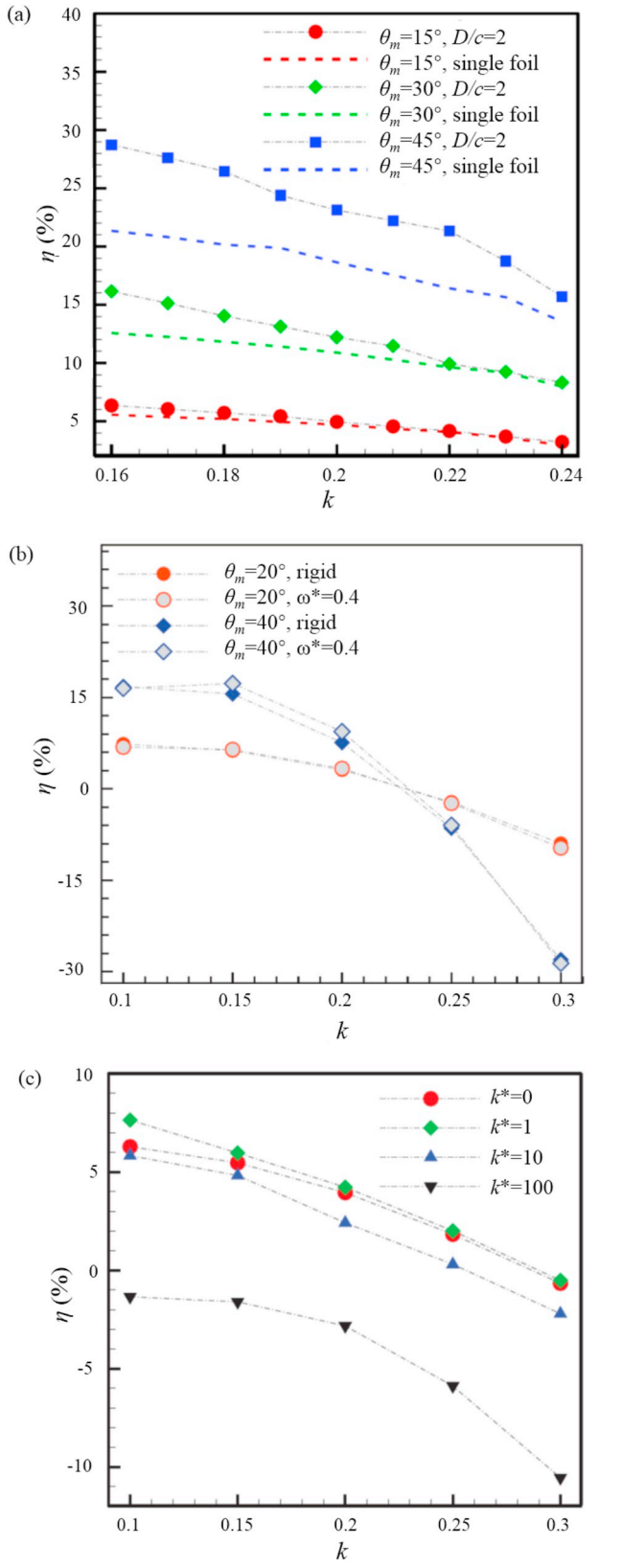

Fig. 19. Comparison of energy extraction efficiency (η) for a semi-active flapping foil (a) with the auxiliary foil (Wu et al., 2015a), (b) with the flexible tail (Wu et al., 2015c) and (c) with different spring constant (Wu et al., 2014). θ_m, D/c, ω^* and k^* represent the pitching amplitude, the distance between flapping foil and auxiliary foil D non-dimensionlized by chord length c, the flexibility of the tail and non-dimensionlized spring constant, respectively.

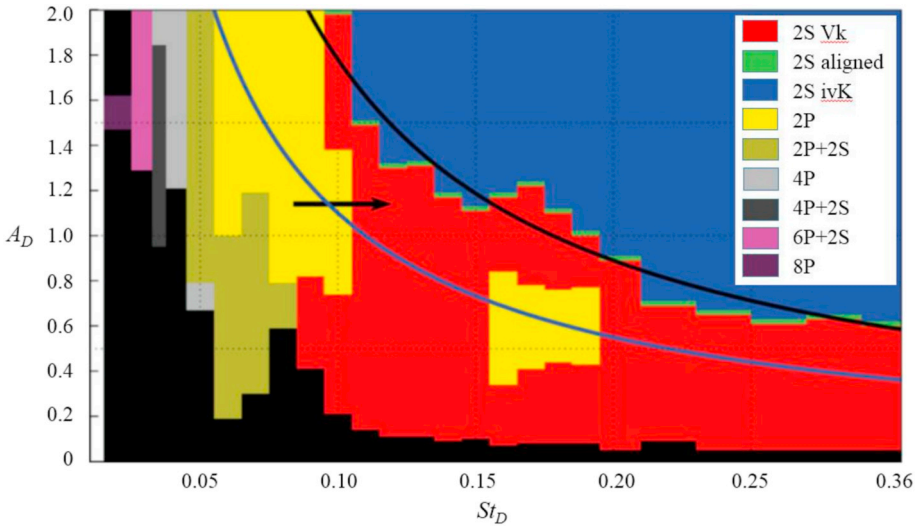

Fig. 20. The map of flow structure for the flapping foil (Schnipper et al., 2009). The black regions represent no periodic wake observed. In the legend, 'vK' is for von Kármán vortex street and 'ivK' is for inverted von Kármán vortex street. 'S' represents a single vortex and 'P' represents a pair of vortices of opposite signs.

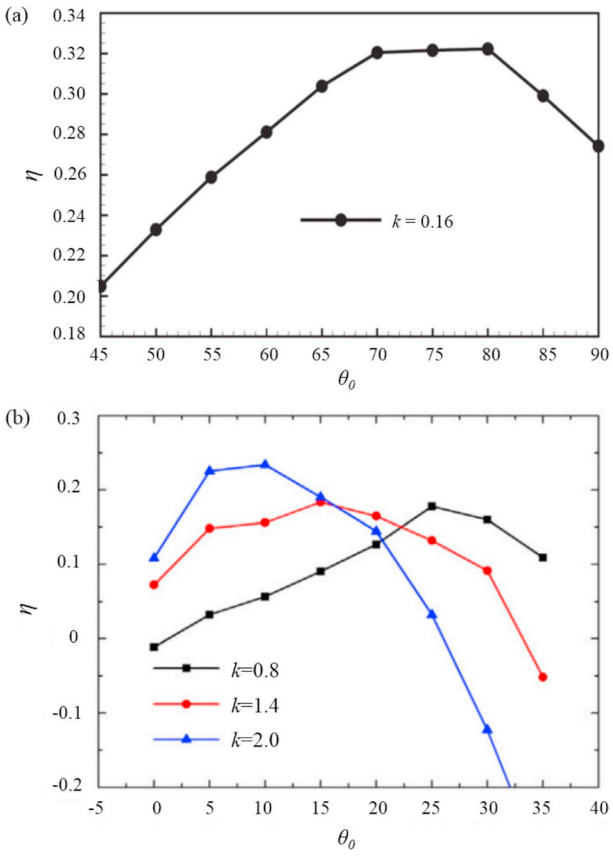

Fig. 21. Variation of energy harvesting efficiency with pitching amplitude θ_0 for (a) $k = 0.16$ (Teng et al., 2016), (b) different $k = 0.8, 1.4, 2.0$ (Xie et al., 2014).

depends on both St and aspect ratio, and the propulsion efficiency is sensitive to aspect ratio less than 0.83. In nature, the reason why tuna can swim at a high speed for a long time in water is associated with its body structure (Zhu et al., 2002). Its body has low aspect ratio and good flexibility. The interaction between vortices generated by the body of tuna and the fin results in two different propulsion modes: high thrust mode and high propulsion efficiency mode.

Simpson et al. (2008) conducted experiments on a flapping foil with aspect ratios from 4.1 to 7.9 and found that the energy harvesting efficiency increases with increasing aspect ratio. The maximum efficiency is 43% at an aspect ratio of 7.9. Deng et al. (2014) investigated the effect of aspect ratios from 1 to 8 on the energy harvesting efficiency of an oscillating foil using DNS. They pointed out that the three-dimensional effect arises at aspect ratios less than 4 and too small aspect ratio can reduce energy harvesting efficiency. Kim et al. (2017) used an oscillating hydrofoil with a rectangular cross section to carry out the experiment on energy harvesting performance at three different aspect ratios (AR = 2.5, 3.5 and 4.5). They found that the total efficiency increases with aspect ratio over the parameter domain considered in their study, which is similarly to the previous numerical work of Kinsey and Dumas (2012) and experimental work of Simpson et al. (2008).

5. Concluding remarks

Since the first observation of lift and thrust generated by a flapping winging by Knoller (1909) and Betz (1912), more and more attentions have been paid to the researches on the fluid dynamics of a flapping foil. This paper performs a comprehensive review of the-state-of-the-art of aero/hydrodynamics of the flapping foil. Firstly, a brief description of the flapping foil is presented in terms of relevant parameters, motion modes and research contents. The contents of all the researches are roughly categorized into four different aspects: flow structure, hydrodynamic characteristics, energy harvesting and bionics problems. This section aims to promote an overall understanding of the flapping foil. In this review, bionics problems based on the flapping foils are not introduced too much but detailed summaries on fish swimming and birds flying are reviewed by Rozhdestvensky and Ryzhov (2003), Wu (2010), Eloy (2012) and Wang et al. (2016b).

Furthermore, the papers in recent decades using experimental or numerical methods are reviewed. Environment and kinematic parameters and other geometric parameters of this part help clarify the settings of the research contents. Through the analysis of data, a rough range of some influencing parameters involved in the flapping foil are also summarized and the results of experimental and numerical studies are compared with each other. At last, the common laws of Reynolds number, reduced frequency, amplitude of foil motion and three-dimensional effect are summarized, respectively. However, there is no apparent law for these parameters on some problems such as the influence of motion amplitude on hydrodynamic coefficient and energy extraction efficiency. It is worth noting that the relevant researches on

Table 1
Experimental works.

Investigators	Equipment	Visualization & velocity measurement	Foil cross-section	Flexibility of foil	St	Re	k	AR	h_0/c	φ(deg)	θ_0/α_0 (deg)	Mean AOA (deg)	Motion profile	Pivot location X/c
Young et al. (2019)	Cyber–Physical Fluid Dynamics (CPFD) Facility	PIV	NACA0012	rigid	–	10000	1.6, 2.4, 3.2	2D	0.10, 0.25, 0.40	–	–	0, 5, 10, 15, 20	sinusoidal	–
Dash et al. (2018)	re-circulating channel	–	ellipse	rigid	0.1–0.9	5000	–	2D (10)	0.75	90	$\alpha_0 = 10,15,20$	0	sinusoidal & non-	1/2
Buren et al. (2017)	free-surface recirculating water channel	PIV	teardrop	rigid	0.05–0.4 (St_A)	4870	heave:1.2 pitch:0.87	2D (3.5)	0.0625–0.1875	–	$\theta_0 = 3$-15	0	sinusoidal & non-	–
Mackowski and Williamson (2017)	Cornell-AFOSR hybrid water channel	–	NACA0012	rigid	–	16600	0–10	2D	induced	–	$\theta_0 = 8$	0	sinusoidal	-1–2
Moubogha et al. (2017)	water channel	PIV	rectangle (flat plate)	rigid	–	2000	1.5–5	2D	–	–	$\theta_0 = 10$	0	sinusoidal	1/3
Kim et al. (2017)	free-surface water flume	PIV	ellipse and rectangle	rigid	–	50000	0.08–0.2	2.5, 3.5, 4.5	0.5–1.0	90	$\theta_0 = 45$-85	0	sinusoidal	1/2
Cleaver et al. (2016)	closed-loop water tunnel	DIC and volumetric velocimetry measurements	rectangle (flat plate)	flexible	0–2.025	10000	–	1.5, 3, 6	0.15	–	$\alpha_0 = 15$		sinusoidal	0 (root)
Lua et al. (2016)	re-circulating channel	–	ellipse	rigid	0.1–0.8	5000		2D (10)	0.75	90	$\alpha_0 = 10,15,20$	0	sinusoidal	1/2
Tian et al. (2016)	closed-circuit low-speed wind tunnel	DPIV	NACA0012	rigid	–	3400	3.8–13.2	2D (3)	–	–	$\alpha_0 = 5$	0	sinusoidal	0.16–0.52
Ashraf et al. (2015)	low Reynolds number water channel	PIV	NACA0015	rigid	–	2900	1.82–10.92	2D (6.4)	–	–	$\alpha_0 = 5$	0	sinusoidal	0 (leading edge)
Lu et al. (2015)	large scale wind tunnel	PIV	NACA0012	rigid	–	3500	0.05–0.5	2D (2.5)	1.67, 2.5, 3.33	–	$\theta_0 = 40, 50$	0	sinusoidal	2/3
Mackowski and Williamson (2015)	Cornell-AFOSR hybrid water channel	PIV	NACA0012	rigid	0.1–0.45 (St_A)	12000 16000	0–12	2D (2.4)	–	–	$\theta_0 = 2$-32	0	sinusoidal	1/4
Monnier et al. (2015)	free-surface closed-return water tunnel	hydrogen (H2) bubbles and PIV	head: NACA0036 tail: rectangle	head:rigid tail: flexible	0.01–0.58	2010	1.41–7.03	2D (4.23)	–	–	$\theta_0 = 1$-10	0	sinusoidal	1/4
Sadeghi et al. (2015)	low speed wind tunnel	hot-wire anemometer	Eppler361	rigid	–	50000	0.1	2D (3.1)	–	–	$\theta_0 = 8$-15	2.5	sinusoidal	1/2
Bøckmann and Steen (2014)	deep towing tank	–	NACA0015	rigid	0.12, 0.18. 0.23	200000	–	9.65	0.64	90	$\theta_0 = 0$-18	0	sinusoidal	1/4
Calderon et al. (2014)	water tunnel	PIV and volumetric three-component velocimetry laser system	NACA0012	rigid	0–4.050 0–2.025	5000 10000	0–12.72 0–6.36	3	0.15	–	–	0	sinusoidal	–
Panah and Buchholz (2014)	free-surface water channel	fluorescein dye and PIV	rectangle (flat plate)	rigid	0.1–0.6(St_A)	10000	0.39–4.7	2D	0.2, 0.3, 0.4	–	–	0	sinusoidal	–
Cleaver et al. (2013)	closed-loop water channel	PIV	NACA0012	rigid	0–0.8	40000	–	2D (3.77)	0.1–0.5	–	–	0	sinusoidal	–
Dewey et al. (2013)	closed-loop, free-surface water channel	optical encoder (angular velocity)	rectangle (flat plate)	flexible	–	7200	2.3–18.8	0.5, 1.0, 1.5, 2.0, 2.4	–	–	$\theta_0 = 0$–14.32	0	sinusoidal	0 (leading edge)

(*continued on next page*)

Table 1 (*continued*)

Investigators	Equipment	Visualization & velocity measurement	Foil cross-section	Flexibility of foil	St	Re	k	AR	h_0/c	φ(deg)	θ_0/α_0 (deg)	Mean AOA (deg)	Motion profile	Pivot location X/c
Panah et al. (2013)	free-surface water channel	SPIV	rectangle (flat plate)	rigid	0.2	10000	–	1, 2, 4	0.3	–	–	0	sinusoidal	–
Hu et al. (2013)	closed-circuit low-speed wind tunnel	PIV	NACA0012	rigid	0.11–0.63 (St_A)	3500	–	2D (2.89)	5.1–17.9	–	$\theta_0 = 5, 10, 15$	0, 2, 5, 7	sinusoidal	0 (root)
Visbal et al. (2013)	large-scale, free-surface water channel	SPIV and PIV	rectangle (flat plate)	rigid	–	10000	1	2	0.25	–	induced	8	sinusoidal	–
Baik and Bernal (2012)	low-turbulence water channel	dye flow visualization and PIV	SD7003 rectangle (flat plate)	rigid	0.08	10000 30000 60000	0.25	2D	0.5	90	$\theta_0 = 8.42$	0	sinusoidal	–
Boiron et al. (2012)	water tunnel	DPIV	NACA0012	rigid	0.15–0.6	4000	0–0.6	2D	0.75	90	$\theta_0 = 5.22$–47.53	0	sinusoidal	3/10
Cleaver et al. (2012)	free-surface closed-loop water tunnel	PIV	NACA0012	rigid	0–3.0	10000	–	2D	0.025–0.2	–	–	0	sinusoidal	–
Fenercioglu and Cetiner (2012)	closecircuit, free-surface, large scale water channel	DPIV	SD7003	rigid	0.05–1.0 (St_A)	825–13700	0.16–6.26	2D (3)	0.25–1.0	90	$\theta_0 = 8.6$	8	sinusoidal	1/4
Panah and Buchholz (2012)	free-surface water channel	DPIV	rectangle (flat plate)	rigid	0.1–0.6(St_A)	10000	–	2D	0.2, 0.3, 0.4	–	–	0	sinusoidal	–
Yu et al. (2012)	closed-circuit low-speed wind tunnel	PIV	NACA0012	rigid	0.1–0.37 (St_A)	3340	5–17.6	2D (2.875)	–	–	$\theta_0 = 5$	0	sinusoidal	0 (root)
Buchholz and Panah (2011)	free-surface water channel	DPIV	rectangle (flat plate)	rigid	0.1, 0.3, 0.5 (St_A)	10000	–	2D	0.2, 0.3, 0.4	–	–	0, 5, 10	sinusoidal	–
Sadeghi et al. (2011)	subsonic wind tunnel	hot-wire anemometer	Eppler361	rigid	–	–	0.182	2D (3.1)	–	–	$\theta_0 = 8, 10, 15$	0, 2.5, 5, 10	sinusoidal	1/4
Baik et al. (2010)	low-turbulence water channel	dye flow visualization and PIV	rectangle (flat plate)	rigid	0..1, 0.15, 0.20	10000	0.314, 0.419, 0.471, 0.628	2D	0.250, 0.375, 0.500	90	$\theta_0 = 3.39$, 11.18, 18.09	8	sinusoidal	0 (root)
Kim and Chang (2010)	low speed wind tunnel	smoke-wire visualization,	NACA0012	rigid	–	23000 33000 48000	0.1	2D	–	–	$\theta_0 = 6$	0	sinusoidal	1/4
Münch et al. (2010)	The EPFL High-Speed CavitationTunnel	–	NACA0009	rigid	–	500000–1500000	0.04–1.25	2D	–	–	$\theta_0 = 2$	0	sinusoidal	1/2
Bohl and Koochesfahani (2009)	closed-return water tunnel	Molecular tagging velocimetry (MTV)	NACA0012	rigid	–	12600	4.1–11.5	2D (4)	–	–	$\theta_0 = 2$	0	sinusoidal	1/4
Sadeghi and Mani (2009)	low speed wind tunnel	hot-wire anemometer	Eppler361	rigid	–	50000	0.182	2D (3)	–	–	$\theta_0 = 8$	0–10	sinusoidal	1/2
Schnipper et al. (2009)	gravity-driven, vertically flowing soap film	soap film	teardrop	rigid	0–0.3	220, 440	–	2D	–	–	$A_D = 0$-2	–	sinusoidal	–
Srigrarom and Chai (2009)	low speed wind tunnel	dye flow visualization and PIV	SD7003 SD8020	rigid	0.1–0.9	13000-16000	–	2D (2.67)	–	–	$\theta_0 = 10$-40	0	sinusoidal	1/4
Buchholz and Smits (2008)	water tunnel	dye flow visualization and DPIV	rectangle (flat plate)	rigid	0–1.0	640 10000	–	0.54–2.38	–	–	Ac = 0.17, 0.26, 0.34	0	sinusoidal	0 (root)

(*continued on next page*)

Table 1 (*continued*)

Investigators	Equipment	Visualization & velocity measurement	Foil cross-section	Flexibility of foil	St	Re	k	AR	h_0/c	φ(deg)	θ_0/α_0 (deg)	Mean AOA (deg)	Motion profile	Pivot location X/c
Godoy-Diana et al. (2008)	hydrodynamic tunnel	PIV	teardrop	rigid	0–0.5	255	–	2D (4)	–	–	$A_D = 0.36–2.8$	0	sinusoidal	0 (leading edge)
Heathcote et al. (2008)	free-surface closed-loop water tunnel	PIV	NACA0012	flexible and rigid	0-1 (St_A)	10000 20000 30000	0–7	4	0.175	–	–	–	sinusoidal	–
Ol et al. (2008)	horizontal freesurface water tunnel	PIV	SD7003	rigid	–	10000	–	2D (3)	0.092	90	$\theta_0 = 21.5$	4	sinusoidal and non-	1/4
Simpson et al. (2008)	small tank	–	NACA0012	rigid	0.2–0.6 (St_A)	13800	–	4.1, 5.9, 7.9	1.23	90	$\alpha_0 = -11–57$	–	sinusoidal	1/4
Srigrarom and Vincent (2008)	closed-loop water tunnel	dye flow visualization and PIV	SD8020	rigid	0–1.2	4176–20496	–	2D (2.67)	0.833	–	$\theta_0 = 10$-45	0–45	sinusoidal	–
von Ellenrieder and Pothos (2007)	recirculating water channel	PIV	NACA0012	rigid	0.174–0.781	2700	–	2D	0.215	–	–	0	sinusoidal	–
Lua et al. (2007)	recirculating water channel	DPIV	ellipse	rigid	0.0919, 0.16, 0.276 (St_A)	1000	0.1–2.0	2D	0–3	–	–	–	sinusoidal	–
Parker et al. (2007)	water tunnel	PIV	NACA0030	rigid	0.35	600	–	3	0.5	90	$\theta_0 = 5$	0	sinusoidal	1/4
Buchholz and Smits (2005)	water channel	DPIV	rectangle (flat plate)	rigid	0.2–0.25	640	1.4, 2.6, 3.9	0.54	–	–	$A_C = 0.17$	0	sinusoidal	0 (leading edge)
Schouveiler et al. (2005)	tow tank	dye flow visualization	NACA0012	rigid	0.10–0.45	40000	–	2D (6)	0.75	90	$\alpha_0 = 10$-35	0–45	sinusoidal	1/3
Hover et al. (2004)	MIT Department of Ocean Engineering Testing Tank	–	NACA0014	rigid	0.2–0.8	30000	–	2D (6)	1	90	$\alpha_0 = 10$-35	0	sinusoidal and non-	1/3
von Ellenrieder et al. (2003)	re-circulating water tunnel	dye flow visualization	rectangle (flat plate)	rigid	0.2–0.4	164	–	3	0.5	60–120	$\theta_0 = 0$-20	0	sinusoidal	1/4
Read et al. (2003)	MIT Department of Ocean Engineering Testing Tank	–	NACA0012	rigid	0.2–0.6	40000	–	2D (6)	0.75, 1.00	70–110	$\alpha_0 = 10$-40	0	sinusoidal and non-	1/3
Chang and Yoon (2002)	closed-circuit wind tunnel	hot-wire anemometer	NACA0012 NACA4412	rigid	–	190000	0.1	2D (3.4)	–	–	$\theta_0 = 6$	0	sinusoidal	1/4
Kuo and Hsieh (2001)	re-circulating water tunnel	LDV	NACA0012	rigid	–	1200	4.05	2D	–	–	$\theta_0 = 5$	15	sinusoidal	1/3
von Ellenrieder et al. (2001)	re-circulating water tunnel	dye flow visualization	teardrop	rigid	0.2–0.4	164	–	2.1	1	–	–	–	sinusoidal	–
Lai and Platzer (1999)	water tunnel	dye flow visualization and LDV	NACA0012	rigid	0.18–9.3 (St = kh)	500–21000	0–130	2D (3.7)	0.0125–0.6	–	–	–	sinusoidal	–
Jones et al. (1999)	Naval Postgraduate School water tunnel	–	Helicopterrotor blade	rigid	–	30000	1.5–2.5	5.6	0.3	90	$\theta_0 = 25, 30$	0	sinusoidal	1/2
Jones and Platzer (1999)	Naval Postgraduate School low-speed wind-tunnel	a pitot-static tube (and LDV)	NACA0014	rigid	–	18000-80000	0.1–1.0	20	0.32, 0.34, 0.4	−90	$\theta_0 = 0, 3.5, 5.0$	0, 6, 10	sinusoidal	1/2

(*continued on next page*)

Table 1 (*continued*)

Investigators	Equipment	Visualization & velocity measurement	Foil cross-section	Flexibility of foil	St	Re	k	AR	h_0/c	φ(deg)	θ_0/α_0 (deg)	Mean AOA (deg)	Motion profile	Pivot location X/c
Anderson et al. (1998)	MIT Department of Ocean Engineering Testing Tank	DPIV	NACA0012	rigid	0.1–0.45 (St_A)	1100, 40000	0.16–1.41	2D (6)	0.25, 0.5, 0.75	30–110	$\theta_0 = 0$, 7, 15, 30, 45, 60	0	sinusoidal	1/3
Jones et al. (1998)	Naval Postgraduate School Eidetics water tunnel	LDV	NACA0012 NACA0015	rigid	0.3–2.3 (St = kh)	500–50000	3.6–26.1	2D (3.7, 18.5)	0.04–0.65	–	–	–	sinusoidal	–
Myose and Iwata (1996)	water tunnel	dye flow visualization	NACA0011 (sawtooth trailing edge)	rigid	–	28000	0.75, 1.5, 2.25	3D	–	–	$\theta_0 = 2$, 4	0	sinusoidal	1/4
Ohmi et al. (1991)	tall rectangular water tank	–	NACA0012 and ellipse	rigid	–	1500 3000 10000	0.1, 0.5, 1.0	2D	–	–	$\theta_0 = 7$, 15	15, 30	sinusoidal	1/2, 1/3
Koochesfahani (1989)	low speed water channel	LDV	NACA0012	rigid	–	12000	0–12	2D (4.875)	–	–	$\theta_0 = 2$, 4	0	sinusoidal and non-sinusoidal	1/4
Freymuth (1988)	horizontal wind tunnel	–	NACA0015	rigid	–	5200 12000	2.7 2.9	2D	0.2	–	$\theta_0 = 20$	5		1/4

* In the column of AR in Table 1, the number in brackets represent the actual aspect ratio of the 2D foils, which are informed in papers directly.

energy extraction based on the flapping foil have been reviewed by Peng and Chen (2012), Xiao and Zhu (2014), Young et al. (2014) and Rostami and Armandei (2017).

Based on the review of a large amount of researches, it seems that the researches on the hydrodynamic characteristics of the oscillating hydrofoil have been very thorough. However, many problems are still not completely understood, such as how the flapping foil reversing Kármán street, how drag becoming thrust; and how to generate the optimal thrust, propulsive efficiency and energy extraction efficiency from flow field. This reminds us that we need to have an insight into these seemingly "simple questions". Recently, Smits' team found that the wake structures of swimmers have no connection with the integrated swimming performance (Floryan et al., 2019; Smits, 2019). Smits also summarized other five main conclusions from aspects of flexibility, combined motions, viscous effects, aspect ratio and motion profiles, which can improve our understanding of undulatory and oscillatory swimming (Smits, 2019). Hence, the following directions are recommended for future research activities:

i) Due to the complexities of three-dimensional flow, the studies of foils are still focused on two-dimensional structures at low or moderate Reynolds number. This has been far from the real applications, where the effects of three-dimensionality, free stream turbulence and high Reynolds numbers should be considered. The foil always has limited aspect ratio so its flow mechanism could be more complex and its end effect may influence the performance of propulsion and energy extraction. Therefore, a focus should be put on the study of flow characteristics of three-dimensional oscillating foils and the simulations based on real environment parameters in future.

ii) Compared with rotary turbines, the flapping foil designs have some advantages: environment-friendly and less noise; simple structure and easy manufacture; suitable for shallow water area; eco-friendly and less biological damage, etc. However, a systematic comparison between the rotary systems and the flapping foil systems has not yet been investigated. The apparently different wake structures may cause the differences in propulsion efficiency and energy harvesting efficiency. The further researches can perform specific quantitative analysis between the two systems.

iii) The majority of studies are concentrated on single foil devices. A few works discussed the multiple foils in tandem or parallel configuration. The energy harvesting efficiency of oscillating foils in tandem or parallel configuration has been investigated by Kinsey and Dumas (2012) and Karbasian et al. (2015). The propulsive performance of tandem flapping wings has been studied by Akhtar et al. (2007), Gong et al. (2015), Gravish et al. (2015), Pan et al. (2016) and Muscutt et al. (2017). In addition, Kumar and Hu (2010) investigates flow structures in wakes of tandem flapping wings. Peng et al. (2018a,b) studies the propulsion efficiency of two or more self-propelled flapping flexible wings. However, all of above simulations are two-dimensional models. Actually, the idea of "turbine farms" can also be used on flapping foils designs. Moreover, non-sinusoidal oscillating motion, structural flexibility and multiple foils can improve the efficiency. The future researches can focus on the behavior of flapping flexible foil systems in non-sinusoidal oscillating motion in large arrays.

iv) The flapping foil designs are mostly inspired by flying birds and swimming fishes but there are still some "secrets" about them to be discovered. For instance, how birds drive their wings and how fishes flap their fins to generate high efficient thrust are not fully clear. This requires more knowledge of three-dimensional flow control mechanisms, fluid-structure interaction and the vortex structures. The further researches can find out more specific explanations and resources from these animals for real applications.

Table 2

Investigators	Numerical methodology				Foil cross-section	Flexibility of foil	St	Re	k	AR	h_0/c	φ(deg)	θ_0/α_0 (deg)	Mean AOA (deg)	Pitch/plunge motion profile	Pivot location X/c
	Analysis type	Turbulence model	Method	Solving equation												
Boudreau et al. (2019a)	CFD: Star-CCM+	S-A	–	2D incompressible URANS	NACA0015	rigid	–	3900000	0.1–0.3	2D	1	–	induced	0	sinusoidal	1/4
Chao et al. (2019)	CFD: Fluent	–	FVM	2D incompressible unstedy NS equations	NACA0012	rigid	0.1–0.5	255	–	2D	–	–	$A_D = 0.25$–2.5	0	nonsinusoidal	5/46
Lahooti and Kim (2019)	numerical simulation	–	IBM	2D incompressible unstedy NS equations	symmetric Joukowski	rigid	–	1000	0.14	2D	0.5	−90	$\theta_0 = 76.33$	0	sinusoidal	1/3
Lin et al. (2019)	numerical simulation	–	immersed boundary-simplified circular function-based gas kinetic method	2D compressible unstedy NS equations	NACA0012	rigid	–	0–2000	–	2D	0.1–1.0	0–360	Ac = 0.1–1.0	0	sinusoidal	0–1
Sitorus and Ko (2019)	CFD	k-ω Wilcox-Durbin+	–	2D NS equations	NACA0012	rigid	–	1700000	0.025–0.2	2D (6)	1	90	$\theta_0 = 10$-90	0	sinusoidal	1/4
Wang et al. (2019)	CFD: OpenFOAM	SST k-ω	FVM	URANS	NACA0012	rigid	–	100000-500000	–	2D	0.5	–	induced	0	sinusoidal	1/4
Dash et al. (2018)	CFD: Fluent	–	FVM	2D incompressible unsteady NS equations	ellipse	rigid	0.1–0.9	5000	–	2D	0.75	90	$\alpha_0 = 10$, 15, 20	0	sinusoidal and non-	1/2
Andersen et al. (2017)	numerical simulation	–	PVM	a Lagrangian formulation of the 2D vorticity equation	teardrop	rigid	0.05–0.30	2640	–	2D	$A_D = 0$–2.0	–	–	0	sinusoidal	centre of the semicircular leading edge
Wang et al. (2017b)	UCFD	S-A	–	2D incompressible unstedy NS equations	NACA0012	rigid	0.16–0.44	13800	0.16	2D (7.9)	0.5, 1.0, 1.23, 1.5, 2.0	90	$\theta_0 = 66.5$–106.5	0	sinusoidal	1/3
Li et al. (2017)	numerical simulation	–	system identification method	full compressible NS equations	NACA0012	rigid	–	40000	0.5–2.5	2D	0–0.6	0, 90, 180, −90	$\theta_0 = 5$, 10, 20	0	sinusoidal	1/3
Yu et al. (2017)	UCFD	S-A	FVM	3D unsteady compressible NS equations	NACA0012	rigid	–	1000–1600000	–	2D	0.1–0.9	0	$\theta_0 = 3$-19	0	sinusoidal	1/3
Liu et al. (2016)	CFD	–	FVM	equations of unsteady laminar flow	NACA0012	flexible	–	1000	0.05–0.25	2D	1	−90	$\theta_0 = 60.75$	0	sinusoidal	1/4
Lua et al. (2016)	CFD: Fluent	–	FVM	2D incompressible unstedy NS equations	ellipse		0.1–0.8	5000	–	2D	0.75	90	$\alpha_0 = 10$, 15, 20	0	sinusoidal	1/2
Wang et al. (2016c)	UCFD	S-A	–	2D incompressible unstedy NS equations	NACA 4 and 6 series	rigid	0.4	13800	0.16	2D	1.23	90	$\theta_0 = 85.82$	0	sinusoidal	1/3

(*continued on next page*)

Table 2 (*continued*)

Investigators	Numerical methodology				Foil cross-section	Flexibility of foil	St	Re	k	AR	h_0/c	φ(deg)	θ_0/α_0 (deg)	Mean AOA (deg)	Pitch/plunge motion profile	Pivot location X/c
	Analysis type	Turbulence model	Method	Solving equation												
Abdullah Sani et al. (2016)	CFD: Fluent	SST k-ω	user-defined functions (UDFs)	2D incompressible unstedy NS equations	NACA 4 series	rigid	–	1100 500000	0.1–0.2	2D	1	90	$\theta_0 = 76.3$	0	sinusoidal	1/3
Das et al. (2016)	numerical simulation	–	viscous vortex particle method (VVPM)	2D time-dependent incompressible NS equations in the Lagrangian form	NACA0012	rigid	0–1.0	10–2000	–	2D	–	–	$\theta_0 = 2, 5, 8, 12, 16$	0	sinusoidal	1/4
Teng et al. (2016)	CFD: OpenFOAM	–	FVM	2D time-dependent incompressible NS equations	NACA0015	rigid	–	1000	0.12–0.16	2D	–	–	$\theta_0 = 70$-80	0	sinusoidal and non-	1/3
Martín-Alcántara et al. (2015)	CFD: OpenFOAM	–	FVM	2D incompressible unsteady NS equations	ellipse	rigid	0.4–4.0	500	–	2D	0.03–0.6	–	–	−10	sinusoidal	–
Lu et al. (2015)	CFD:CFX	–	–	2D incompressible unsteay NS equations	NACA0012	rigid	–	3500	0.05–0.5	2D	1.67, 2.5, 3.33	–	$\theta_0 = 40, 50$	0	sinusoidal	2/3
Choi et al. (2015)	numerical simulation	–	IBFS	2D incompressible unsteay NS equations	NACA0006	rigid	–	100–500	0–2.5	2D	0–0.8	–	–	5–20	sinusoidal	–
Zhu et al. (2015)	CFD	S-A	–	RANS	NACA0002, 12, 15	rigid	–	10000 13800	0.14, 0.16	2D	1, 1.23	–	$\theta_0 = 85.82$	0	sinusoidal	1/3
Wu et al. (2015b)	numerical simulation	–	IB-LBM	2D incompressible viscous NS equations	NACA0015	flexible tail	0.05–0.25	1100	–	2D	0.5	90	$\alpha_0 = 10, 20$	0	sinusoidal	1/3
Khalid et al. (2015)	numerical simulation	–	IBM	2D incompressible viscous NS equations	ellipse	rigid	0.2–0.8	500	6.283	2D	0.05–0.2	–	–	0	sinusoidal	–
Deng et al. (2015)	CFD: OpenFoam	–	FVM	time-dependent incompressible NS equations	NACA0015	rigid	–	1000	0.08–0.22	2D	–	–	60–90	0	sinusoidal	1/3
Fenercioglu et al. (2015)	CFD: Fluent	–	–	2D unsteady incompressible NS equations	NACA0012	rigid	–	1100	0.8	2D	1.05	90, 110	$\theta_0 = 73$	0	sinusoidal and non-	1/4, 1/2
Cho and Zhu (2014)	CFD: Fluent	–	FVM	2D NS equations	NACA0012	rigid	–	200	0.06–2.00	2D	1	90	$\theta_0 = 75$	0	sinusoidal	1/3
Deng et al. (2014)	CFD: OpenFoam	–	FVM	time-dependent incompressible NS equations	NACA0015	rigid	0.4	1100	0.163	1–8	1.23	90	$\theta_0 = 81.5$	0	nonsinusoidal	1/3
Lu et al. (2014)	CFD: CFX	–	–	2D unsteady incompressible NS equations	NACA0012	rigid	0.05–0.4	10000	–	2D	0.8	90	$\alpha_0 = 15$	0	nonsinusoidal	1/3
Politis and Tsarsitalidis (2014)	numerical simulation	–	3D Unsteady Boundary Element	–	NACA0012	rigid	0.1–0.7	2020000	–	2, 4, 6	0.5, 1.0, 1.5, 2.0	75, 90	$\theta_0 = 5$-50	0	sinusoidal	1/10, 1/3

(*continued on next page*)

Table 2 (*continued*)

Investigators	Numerical methodology				Foil cross-section	Flexibility of foil	St	Re	k	AR	h_0/c	φ(deg)	θ_0/α_0 (deg)	Mean AOA (deg)	Pitch/plunge motion profile	Pivot location X/c
	Analysis type	Turbulence model	Method	Solving equation												
			Method (UBEM)													
Wu et al. (2014)	numerical simulation	–	IB-LBM	2D unsteady incompressible NS equations	NACA0015	rigid	–	1100	0.1–0.3	2D	1	–	$\theta_0 = 15\text{-}45$	0	sinusoidal	1/3
Xie et al. (2014)	CFD: CFX	–	–	2D unsteady incompressible and viscous flow solver	ellipse	rigid	–	10000	0.4–2.8	2D	1	90	$\theta_0 = 0\text{-}40$	90	sinusoidal	1/2
Zaman et al. (2014)	CFD: Fluent	–	–	2D NS equations	NACA0012	rigid	–	500	8–16	2D	–	–	$\theta_0 = 10\text{-}58$	0	sinusoidal and non-	–
Visbal et al. (2013)	numerical simulation	–	ILES	3D unfiltered full compressible NS equations	rectangle (flat plate)	rigid	–	1000–20000	1	2	0.25	–	–	8	sinusoidal	–
Mantia and Dabnichki (2013)	numerical simulation	–	BEM	–	NACA0012	rigid	0.1–0.5	40000	–	2D	0.75	90	$\alpha_0 = 15$	0	sinusoidal	1/3
Elarbi (2013)	CFD: Fluent	–	FVM	3D unsteady NS equations	NACA0012	rigid	0.0869–0.3186	30000	0.2–3	3D	0.075–0.275	–	–	0	sinusoidal	–
Lu et al. (2013a)	CFD: CFX	–	FVM	2D unsteady incompressible viscous NS equations	NACA 4 series	rigid	–	13500	6–18	2D	–	–	$\theta_0 = 5\text{-}30$	0	sinusoidal and non-	1/4
Lu et al. (2013b)	CFD: CFX	SST k-ω	FVM	URANS	NACA0012	rigid	–	135000	0.1, 0.2	2D	–	–	$\theta_0 = 5, 10, 15$	0	sinusoidal and non-	1/4
Yu et al. (2013)	numerical simulation	–	spectral difference (SD) method	2D unsteady compressible NS equation	NACA 4 series	rigid	0.3, 0.45	1200	1.0, 3.5	2D	–	75	$\theta_0 = 20$	0	sinusoidal	1/3
Esfahani et al. (2013)		–	–	–	teardrop	rigid	0.2–0.7	30000-500000	–	6	0.5–1.0	90	$\alpha_0 = 15$	0	sinusoidal and non-	–
Liu et al. (2013)	CFD	k-ω	FVM	URANS	NACA0012	flexible	–	1000000	0.05–0.25	2D	0.5	−90	$\alpha_0 = 0, 5, 10$	0	sinusoidal	1/3
Kinsey and Dumas (2012)	CFD: Fluent	S-A	FVM	URANS	NACA0015	rigid	–	500000	0.04–20	2D	0.75, 1.0	90	$\theta_0 = 62, 67, 70, 75$	0	sinusoidal	1/3
Medjroubi et al. (2012)	CFD	–	Spectral/hp Element Method (SEM)	3D unsteady incompressible viscous NS equations	NACA0012	rigid	–	10000	1.96–7.85	2D	0.001–0.1	–	–	0	sinusoidal	–
Dai et al. (2012)	numerical simulation	–	IBM	3D incompressible viscous NS equations	rectangle (flat plate)	rigid and flexible	0.1–0.7	640	1, 2	0.54	–	–	$\theta_0 = 12$	0	sinusoidal	leading edge
Boiron et al. (2012)	CFD	–	FEM	3D incompressible NS equations	NACA0012	rigid	0.15–0.6	4000	0–0.6	2D	0.75	90	$\alpha_0 = 20$	0	sinusoidal	3/10
Zheng and Wei (2012)	numerical simulation	–	IBM	2D incompressible NS equations	NACA0012	rigid	0.96, 1.08, 1.2	200–500	5.0–10.0	2D	0.12, 0.16. 0.24	–	–	0	sinusoidal	–
Ashraf et al. (2012)	CFD: Fluent	–	–	2D amd 3D unsteady incompressible NS equations	NACA0012	rigid	0.5, 1.0, 1.25, 1.5	20000	0.25, 1.0, 4.0, 10.	2D and 0.2	0.25–1.5	–	–	0	sinusoidal	–
He et al. (2012)		–	IBM		teardrop	rigid		255	–	2D	–	–		0	sinusoidal	–

(*continued on next page*)

Table 2 (*continued*)

Investigators	Numerical methodology				Foil cross-section	Flexibility of foil	St	Re	k	AR	h_0/c	φ(deg)	θ_0/α_0 (deg)	Mean AOA (deg)	Pitch/plunge motion profile	Pivot location X/c
	Analysis type	Turbulence model	Method	Solving equation												
	numerical simulation			2D incompressible NS equaions			0.10, 0.22, 0.30, 0.40						$A_D = 0.36$, 0.71, 1.07, 1.77, 2.80			
Li and Lu (2012)	numerical simulation	–	IB-LBM	3D incompressible NS equations	rectangle (flat plate)	rigid	0.4, 0.6, 0.8	100, 200, 500, 1000	–	0.5–2.0	0.5	–	$\theta_0 = 30$	0	sinusoidal	leading edge
Yu et al. (2012)	CFD	–	spectral difference (SD) method	2D unsteady compressible NS equations	NACA0012	rigid	0.1–0.37	3340	5.0–17.6	2D	–	–	$\theta_0 = 5$, 10, 15	0	sinusoidal	–
Xiao et al. (2012)	CFD	–	FVM	2D unsteady compressible NS equations	NACA0012	rigid	0.05–0.5	10000	–	2D	0.5, 1.0	90	$\alpha_0 = 10$, 20	0	sinusoidal and non-	1/3
Ashraf et al. (2011a)	CFD: Fluent	S-A	–	2D unsteady incompressible NS equations	NACA series	rigid	–	200,2000,20000, 2000000	2	2D	0.25, 0.5	90	$\theta_0 = 15$, 30	0	sinusoidal	1/3
Medjroubi et al. (2011)	CFD	–	Spectral/hp Element Method (SEM)	2D viscous incompressible NS equations	NACA0012	rigid	–	800, 1600, 4500, 8000,	–	2D	0.1047, 0.7958	–	–	12, 20	sinusoidal	–
Liang et al. (2011)	CFD	–	spectral difference (SD) method	2D unstesady NS equations	NACA0012	rigid	0.46, 1.5	252, 500, 1000, 1850	0.835, 3.09, 5.01, 6.68	2D	0.08, 0.12	–	$\theta_0 = 2$, 4	0	sinusoidal	1/4
Shao et al. (2010)	numerical simulation	–	IBM	incompressible viscous NS equations	NACA0012	rigid	0.35, 0.60	200	–	1.0–5.0	0.5	90	$\theta_0 = 30$	0	sinusoidal	–
Münch et al. (2010)	CFD: CFX	SST k-ω k-ε	FVM	incompressible URANS	NACA0009	rigid	–	500000–1500000	0.02–100	2D	–	–	$\alpha_0 = 2$	0	sinusoidal	1/2
Bansmer et al. (2010)	CFD	Menter-Baseline k-ω	FVM	URANS	SD04	rigid and flexible	–	100000	0.2	2D	0.5	90	$\alpha_0 = 4$	4	sinusoidal	1/4
Hutchinson et al. (2010)	CFD: CFX	SST	–	–	NACA0009, 0015	rigid	–	2800000, 9389000	0.188,0.785, 1.57, 3.14	2D	–	–	$\theta_0 = 2$, 5, 10	0	sinusoidal	1/2
Amiralaei et al. (2010)	CFD: OpenFOAM	–	FVM	2D incompressible NS	NACA0012	rigid	–	555, 1000, 2000, 5000	0.1, 0.125, 0.17, 0.25	2D	–	–	$\theta_0 = 2$, 4, 6, 8, 10	15	sinusoidal	1/4
Thaweewat et al. (2009)	numerical simulation	–	–	–	ellipse	rigid	0.02–0.75	150	–	2D	0.5–3.0	90	0–45	0–75	sinusoidal	1/2
Kang et al. (2009)	CFD	SST	–	2D RANS	SD7003	rigid	0.08	10000-60000	0.25	2D	–	90	–	–	sinusoidal	–
Xiao and Liao (2009)	CFD	k-ω	–	URANS	NACA0012	rigid	–	10000	3.0–14.0	2D	–	–	$\theta_0 = 2$, 4, 6	0	sinusoidal and non-	1/4
Visbal (2009)	numerical simulation	–	ILES	full compressible NS equations	SD7003	rigid	–	10000, 40000,60000	3.93, 10	2D and 0.2	0.005–0.04, 0.05	–	–	4, 14	sinusoidal	–
Shin et al. (2009)	numerical simulation	–	hybrid Cartesian/ immersed boundary method	2D unsteady incompressible NS equations	NACA0012	rigid	–	1100	0.2, 0.225	2D	1	90	$\theta_0 = 40$	0	sinusoidal	1/4
Sarkar and Singasani (2009)	numerical simulation	–	–	2D incompressible NS equations	NACA0012	rigid	–	10000	7.86	2D	0.05	–	$\theta_0 = 21.5$	0, 4, 8	sinusoidal	–
Kinsey and Dumas (2008)	CFD: Fluent	–	FVM	–	NACA0015	rigid	–	1100	0–0.25	2D	1	90	$\theta_0 = 0$-90	0	sinusoidal	1/3

(*continued on next page*)

Table 2 (*continued*)

Investigators	Numerical methodology				Foil cross-section	Flexibility of foil	St	Re	k	AR	h_0/c	φ(deg)	θ_0/α_0 (deg)	Mean AOA (deg)	Pitch/plunge motion profile	Pivot location X/c
	Analysis type	Turbulence model	Method	Solving equation												
Ol et al. (2008)	numerical simulation	–	2D IBM	2D incompressible NS equations	SD7003	rigid	–	300–1200	–	2D	0.092	90	$\theta_0 = 21.5$	4	sinusoidal and non-	1/4
Lian et al. (2008)	numerical simulation	SST	–	RANS	SD7003	rigid	–	60000	0.25	2D	0.5	90	$\theta_0 = 8.42$	8	sinusoidal	1/4
Young and Lai (2007)	numerical simulation	–	–	2D compressible NS equations	NACA0012	rigid	–	20000	1.0–10.0	2D	0.00025–0.500	–	–	0	sinusoidal	–
Kaya and Tuncer (2007)	numerical simulation	B-L	–	RANS	NACA0012	rigid	–	10000	1	2D	0.5	41.4–90.3	$\theta_0 = 8.5$–21.5	0	sinusoidal and non-	1/2
Dong et al. (2006)	numerical simulation	–	IBM	3D unsteady incompressible viscous NS equations	ellipse	rigid	0.3–1.2	100, 200, 400	–	1.27, 2.55 5.09, ∞	0.5	–	$\theta_0 = 30$	0, 10, 20, 30	sinusoidal	1/2
Miao and Ho (2006)	CFD: Fluent	–	FVM	2D unsteady viscous NS equations	NACA0014	flexible	–	100, 1000, 10000	1.0–6.0	2D	0.4	–	–	0	sinusoidal	–
Lee et al. (2006)	numerical simulation	baseline SST k–ω	–	2D unsteady incompressible NS equations	NACA series	rigid	–	5000, 12000	1–12	2D	0.1–0.4, 2	90	$\theta_0 = 20, 30, 40$	0	sinusoidal	1/4
Tuncer and Kaya (2005)	numerical simulation	B-L	–	2D unsteady RANS	NACA0012	rigid	–	10000	1	2D	0.45–2.11	82.4–103.4	$\theta_0 = 15.4$–36.6	0	sinusoidal	1/2
Young and Lai (2004)	numerical simulation	B-L	–	2D unsteady compressible RANS	NACA0012	rigid	–	10000, 20000, 40000, 80000	2, 4, 6, 8	2D	0.0125, 0.025, 0.05, 0.075	–	–	0	sinusoidal	–
Pedro et al. (2003)	CFD	–	FVM	2D unsteady incompressible NS equations	NACA0012	rigid	0.1–0.7	1100	0–20	2D	0.5, 1.0	30–115	$\theta_0 = 5$-50	0	sinusoidal	–
Ramamurti and Sandberg (2001)	numerical simulation	–	–	2D incompressible NS equations	NACA0012	rigid	0.03	12000 1100	0-14 0.3, 0.45	2D	1	30–140	$\theta_0 = 2, 4$ $\theta_0 = 15, 30$	0	sinusoidal	–
Liu and Kawachi (1998)	CFD	–	–	3D incompressible unsteady NS equations	hawkmoth	rigid	–	1700	0.167–0.500	5.3	1.0–3.0	−90	$\theta_0 = 42$	0	sinusoidal	root
Jones and Platzer (1997)	numerical simulation	–	2D unsteady potential-flow panel code	unsteady inviscid incompressible two-dimensional flows	NACA0012	rigid	–	12000	0–20	2D	0.1, 0.2, 0.4	0–360	$\theta_0 = 0$-30	0	sinusoidal	1/4
Visbal and Shang (1989)	numerical simulation	–	–	2D compressible NS equations	NACA0015	rigid	–	10000	0.1–0.6	2D	–	–	$\theta_0 = 60$	0	sinusoidal	0, 1/4, 1/2, 3/4

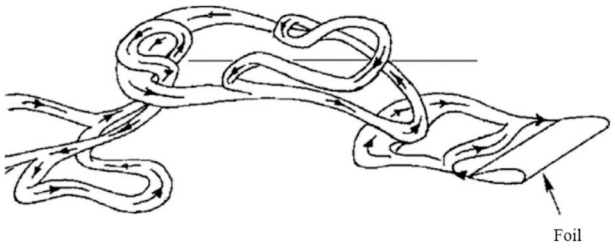

Fig. 22. Three-dimensional vortex structure of a NACA0030 foil at aspect ratio of 3 (von Ellenrieder et al., 2003).

v) Machine learning is one of the hottest topics at present and many fluid issues are solved in this advanced way. Ling et al. (2016) use deep neural networks to develop Reynolds stress closures for RANS turbulence models.Wan and Sapsis (2018) predict the trajectory of spherical particles in fluid flows through machine learning. Raissi et al. (2019) use deep learning method to discuss the problems of vortex induced vibrations. The further researches can attempt to use deep machine learning to make predictions for aero/hydrodynamic force and wake structure of flapping foils in different flow environments.

With so many questions about flapping foils to be answered and explained, the task can be imagined to be very arduous. Nevertheless, an improved understanding of any aspect of the oscillating foil may have important implications for flow structure, aero/hydrodynamic performance and energy harvesting efficiency based on the foil.

Acknowledgement

The authors would like to thank the supports from Natural Science Foundation of Shanghai (Grant no.19ZR1426300), National Natural Science Foundation of China (Grant nos. 11632011, 51779141), Shanghai Pujiang Program (Grant No. 19PJ1405400), the start-up funding from Shanghai Jiao Tong University (Grant No. WF220501006) and Ministry of Industry and Information Technology of China, Project No. [2016] 546.

References

Abdullah Sani, S.A., Djidjeli, K., Xing, J.T., 2016. Geometrical shape influence on energy harvesting performance of oscillating airfoil. In: Sustainable Energy Conference.
Akhtar, I., Mittal, R., Lauder, G.V., Drucker, E., 2007. Hydrodynamics of a biologically inspired tandem flapping foil configuration. Theor. Comput. Fluid Dyn. 21 (3), 155–170.
Alben, S., Witt, C., Baker, T.V., Anderson, E., Lauder, G.V., 2012. Dynamics of freely swimming flexible foils. Phys. Fluids 24 (5), 109–133.
Amiralaei, M.R., Alighanbari, H., Hashemi, S.M., 2010. An investigation into the effects of unsteady parameters on the aerodynamics of a low Reynolds number pitching airfoil. J. Fluids Struct. 26 (6), 979–993.
Andersen, A., Bohr, T., Schnipper, T., Walther, J.H., 2017. Wake structure and thrust generation of a flapping foil in two-dimensional flow. J. Fluid Mech. 812, R4.
Anderson, J.M., Streitlien, K., Barrett, D.S., Triantafyllou, M.S., 1998. Oscillating foils of high propulsive efficiency. J. Fluid Mech. 360, 41–72.
Ashraf, M.A., Young, J., Lai, J.C.S., 2009. Effect of airfoil thickness, camber and Reynolds number on plunging airfoil propulsion. In: 47th Aerospace Sciences Meeting.
Ashraf, M.A., Young, J., Lai, J.C.S., 2011. Reynolds number, thickness and camber effects on flapping airfoil propulsion. J. Fluids Struct. 27 (2), 145–160.
Ashraf, M.A., Young, J., Lai, J.C.S., Platzer, M.F., 2011. Numerical analysis of an oscillating-wing wind and hydropower generator. AIAA J. 49 (7), 1374–1386.
Ashraf, M.A., Young, J., Lai, J.C.S., 2012. Oscillation frequency and amplitude effects on plunging airfoil propulsion and flow periodicity. AIAA J. 50 (11), 2308–2324.
Ashraf, I., Agrawal, A., Khan, M.H., Sooraj, P., Srivastava, A., Sharma, A., 2015. Thrust generation and wake structure for flow across a pitching airfoil at low Reynolds number. Sadhana 40 (8), 2367–2379.
Baik, Y.S., Bernal, L.P., 2012. Experimental study of pitching and plunging airfoils at low Reynolds numbers. Exp. Fluid 53 (6), 1979–1992.
Baik, Y.S., Rausch, J., Bernal, L.P., Shyy, W., Ol, M., 2010. Experimental study of governing parameters in pitching and plunging airfoil at low Reynolds number. In: Proceedings of the 48th AIAA Aerospace Sciences Meeting Including the New Horizons Forum and Aerospace Exposition.
Baik, Y.S., Bernal, L.P., Granlund, K., Ol, M.V., 2012. Unsteady force generation and vortex dynamics of pitching and plunging aerofoils. J. Fluid Mech. 709, 37–68.
Bansmer, S., Radespiel, R., Unger, R., Haupt, M., Horst, P., 2010. Experimental and numerical fluid-structure analysis of rigid and flexible flapping airfoils. AIAA J. 48 (9), 1959–1974.
Barannyk, O., Buckham, B.J., Oshkai, P., 2012. On performance of an oscillating plate underwater propulsion system with variable chordwise flexibility at different depths of submergence. J. Fluids Struct. 28, 152–166.
Belibassakis, K.A., 2011. A panel method based on vorticity distribution for the calculation of free surface flows around ship hull configurations with lifting bodies. Sustain. Marit. Trans. Exploit. Sea Resour. 79 (86), 79–86. ROUTLEDGE in association with GSE Research.
Belibassakis, K.A., Filippas, E.S., 2015. Ship propulsion in waves by actively controlled flapping foils. Appl. Ocean Res. 52, 1–11.
Belibassakis, K.A., Politis, G.K., 2013. Hydrodynamic performance of flapping wings for augmenting ship propulsion in waves. Ocean Eng. 72, 227–240.
Belibassakis, K.A., Politis, G.K., Triantafyllou, M.S., 1997. Application of the Vortex Lattice Method to the propulsive performance of a pair of oscillating wing-tails. In: Proceedings of Eighth International Conference on Comp Methods and Experimental Measurements, CMEM'97, Rhodes, Greece.
Betz, A., 1912. Ein Beitrag zur Erklärung des Segelfluges. Zeitschrift für Flugtechnik und Motorluftschiffahrt 3, 269–272.
Birnbaum, W., 1924. Das ebene problem des schlagenden flügels. ZAMM - J. Appl. Math. Mech./Z. Angew. Math. Mech. 4 (4), 277–292.
Birnbaum, W., 1924. Der Schlagflügelpropeller und die kleinen Schwingungen elastisch befestigter Tragflügel. Zeitschrift für Flugtechnik und Motorluftschiffahrt 15, 128–134.
Bøckmann, E., Steen, S., 2013. The effect of a fixed foil on ship propulsion and motions. In: Proceedings of the Third International Symposium on Marine Propulsors, pp. 553–561.
Bøckmann, E., Steen, S., 2014. Experiments with actively pitch-controlled and spring-loaded oscillating foils. Appl. Ocean Res. 48, 227–235.
Bøckmann, E., Steen, S., 2016. Model test and simulation of a ship with wavefoils. Appl. Ocean Res. 57, 8–18.
Bohl, D.G., Koochesfahani, M.M., 2009. MTV measurements of the vortical field in the wake of an airfoil oscillating at high reduced frequency. J. Fluid Mech. 620, 63.
Boiron, O., Guivier-Curien, C., Bertrand, E., 2012. Study of the hydrodynamic of a flapping foil at moderate angle of attack. Comput. Fluid 59, 117–124.
Boudreau, M., Dumas, G., Rahimpour, M., Oshkai, P., 2018. Experimental investigation of the energy extraction by a fully-passive flapping-foil hydrokinetic turbine prototype. J. Fluids Struct. 82, 446–472.
Boudreau, M., Gunther, K., Dumas, G., 2019. Investigation of the energy-extraction regime of a novel semi-passive flapping-foil turbine concept with a prescribed heave motion and a passive pitch motion. J. Fluids Struct. 84, 368–390.
Boudreau, M., Gunther, K., Dumas, G., 2019. Free-pitching flapping-foil turbines with imposed sinusoidal heave. J. Fluids Struct. 90, 110–138.
Boudreau, M., Picard-Deland, M., Dumas, G., 2020. A parametric study and optimization of the fully-passive flapping-foil turbine at high Reynolds number. Renew. Energy 146, 1958–1975.
Bratt, J.B., 1950. Flow Patterns in the Wake of an Oscillating Airfoil. Aeronautical Research Council, R&M, p. 2773.
Buchholz, J.H., Panah, A.E., 2011. Scaling of circulation shed by an oscillating airfoil. In: AIAA Fluid Dynamics Conference and Exhibit.
Buchholz, J.H., Smits, A.J., 2005. On the evolution of the wake structure produced by a low-aspect-ratio pitching panel. J. Fluid Mech. 564, 433–443.
Buchholz, J.H., Smits, A.J., 2008. The wake structure and thrust performance of a rigid low-aspect-ratio pitching panel. J. Fluid Mech. 603, 331–365.
Buren, T.V., Floryan, D., Quinn, D., Smits, A.J., 2017. Nonsinusoidal gaits for unsteady propulsion. Phys. Rev. Fluid 2 (5).
Buren, T.V., Floryan, D., Smits, A.J., 2018. Scaling and performance of simultaneously heaving and pitching foils. AIAA J. 1–12.
Calderon, D.E., Cleaver, D.J., Gursul, I., Wang, Z., 2014. On the absence of asymmetric wakes for periodically plunging finite wings. Phys. Fluids 26 (7), 071907.
Chang, J.W., Yoon, Y.H., 2002. Camber effects on the near wake of oscillating airfoils. J. Aircr. 39 (4), 713–716.
Chao, L.M., Pan, G., Zhang, D., Yan, G.X., 2019. Numerical investigations on the force generation and wake structures of a nonsinusoidal pitching foil. J. Fluids Struct. 85, 27–39.
Chen, Y., Zhan, J., Wu, J., Wu, J., 2017. A fully-activated flapping foil in wind gust: energy harvesting performance investigation. Ocean Eng. 138, 112–122.
Cho, H., Zhu, Q., 2014. Performance of a flapping foil flow energy harvester in shear flows. J. Fluids Struct. 51, 199–210.
Cleaver, D.J., Wang, Z., Gursul, I., 2012. Bifurcating flows of plunging aerofoils at high Strouhal numbers. J. Fluid Mech. 708, 349–376.
Choi, J., Colonius, T., Williams, D.R., 2015. Surging and plunging oscillations of an airfoil at low Reynolds number. J. Fluid Mech. 763, 237–253.
Cleaver, D.J., Calderon, D.E., Wang, Z., Gursul, I., 2013. Periodically plunging foil near a free surface. Exp. Fluid 54 (3).
Cleaver, D.J., Calderon, D.E., Wang, Z., Gursul, I., 2016. Lift enhancement through flexibility of plunging wings at low Reynolds numbers. J. Fluids Struct. 64, 27–45.
Couder, Y., Basdevant, C., 1986. Experimental and numerical study of vortex couples in two-dimensional flows[J]. J. Fluid Mech. 173 (173), 225–251.
Dai, H., Luo, H., de Sousa, P.J.S.A.F., Doyle, J.F., 2012. Thrust performance of a flexible low-aspect-ratio pitching plate. Phys. Fluids 24 (10), 101903.
Das, A., Shukla, R.K., Govardhan, R.N., 2016. Existence of a sharp transition in the peak propulsive efficiency of a low- pitching foil. J. Fluid Mech. 800, 307–326.

Dash, S.M., Lua, K.B., Lim, T.T., Yeo, K.S., 2018. Enhanced thrust performance of a two dimensional elliptic airfoil at high flapping frequency in a forward flight. J. Fluids Struct. 76, 37–59.
Deng, J., Caulfield, C.P., Shao, X., 2014. Effect of aspect ratio on the energy extraction efficiency of three-dimensional flapping foils. Phys. Fluids 26 (4), 043102.
Deng, J., Teng, L., Pan, D., Shao, X., 2015. Inertial effects of the semi-passive flapping foil on its energy extraction efficiency. Phys. Fluids 27 (5), 053103.
Dewey, P.A., Carriou, A., Smits, A.J., 2011. On the relationship between efficiency and wake structure of a batoid-inspired oscillating fin. J. Fluid Mech. 691, 245–266.
Dewey, P.A., Boschitsch, B.M., Moored, K.W., Stone, H.A., Smits, A.J., 2013. Scaling laws for the thrust production of flexible pitching panels. J. Fluid Mech. 732, 29–46.
Dohring, C.M., Platzer, M.F., Jones, K.D., Tuncer, I.H., 1996. Computational and experimental investigation of the wakes shed from flapping airfoils and their wake interference/impingement characteristics. In: Proceedings of the AGARD–FDP Symposium on the Characterisation and Modification of Wakes from Lifting Vehicles in Fluids, AGARD CP-584, vol. 33, pp. 1–9.
Dong, H., Mittal, R., Najjar, F.M., 2006. Wake topology and hydrodynamic performance of low-aspect-ratio flapping foils. J. Fluid Mech. 566, 309.
Duarte, L., Dellinger, N., Dellinger, G., Ghenaim, A., Terfous, A., 2019. Experimental investigation of the dynamic behaviour of a fully passive flapping foil hydrokinetic turbine. J. Fluids Struct. 88, 1–12.
Elarbi, E., 2013. Plunging frequency-amplitude effects on propulsion performance of flapping NACA 0012 wing. In: AIAA Aerospace Sciences Meeting Including the New Horizons Forum and Aerospace Exposition.
Eldredge, J.D., Toomey, J., Medina, A., 2010. On the roles of chord-wise flexibility in a flapping wing with hovering kinematics. J. Fluid Mech. 659, 94–115.
Eloy, C., 2012. Optimal Strouhal number for swimming animals. J. Fluids Struct. 30, 205–218.
Esfahani, J.A., Barati, E., Karbasian, H.R., 2013. Comparative investigations on the effect of angle of attack profile in performance of bio-inspired propulsion (flapping foil). J. Nav. Archit. Mar. Eng. 10 (2).
Esfahani, J.A., Barati, E., Karbasian, H.R., 2015. Fluid structures of flapping airfoil with elliptical motion trajectory. Comput. Fluid 108, 142–155.
Fenercioglu, I., Cetiner, O., 2012. Categorization of flow structures around a pitching and plunging airfoil. J. Fluids Struct. 31, 92–102.
Fenercioglu, I., Zaloglu, B., Young, J., Ashraf, M.A., Lai, J.C.S., Platzer, M.F., 2015. Flow structures around an oscillating-wing power generator. AIAA J. 53 (11), 3316–3326.
Filippas, E.S., Gerostathis, T.P., Belibassakis, K.A., 2018. Semi-activated oscillating hydrofoil as a nearshore biomimetic energy system in waves and currents. Ocean Eng. 154, 396–415.
Floc'h, F., Phoemsapthawee, S., Laurens, J.M., Leroux, J.B., 2012. Porpoising foil as a propulsion system. Ocean Eng. 39, 53–61.
Floryan, D., Van Buren, T., Rowley, C.W., Smits, A.J., 2017. Scaling the propulsive performance of heaving and pitching foils. J. Fluid Mech. 822, 386–397.
Floryan, D., Van Buren, T., Smits, A.J., 2018. Efficient cruising for swimming and flying animals is dictated by fluid drag. In: Proceedings of the National Academy of Sciences, vol. 115, pp. 8116–8118, 32.
Floryan, D., Van Buren, T., Smits, A.J., 2019. Swimmers' Wakes Are Not Reliable Indicators of Swimming Performance. arXiv preprint arXiv:1906.10826.
Freymuth, P., 1988. Propulsive vortical signature of plunging and pitching airfoils. AIAA J. 26 (7), 881–883.
Freymuth, P., 1990. Thrust generation by an airfoil in hover modes. Exp. Fluid 9 (12), 17–24.
Freymuth, P., Bank, W., Finaish, F., 1987. Further visualization of combined wing tip and starting vortex systems. AIAA J. 25 (9), 1153–1159.
Garrick, I.E., 1936. Propulsion of a Flaaping and Oscillating Airfoil. Technical Report. Archive & Image Library.
Gharib, M., Derango, P., 1989. A liquid film (soap film) tunnel to study two-dimensional laminar and turbulent shear flows. Phys. D Nonlinear Phenom. 37 (1), 406–416.
GIauert, M.A.H., 1929. The Force and Moment on an Oscillating Aerofoil. Technical Report 1242. Aeronautical Research Committee, pp. 88–95.
Godoy-Diana, R., Aider, J.L., Wesfreid, J.E., 2008. Transitions in the wake of a flapping foil. Phys. Rev. E - Stat. Nonlinear Soft Matter Phys. 77 (2), 016308.
Gong, W.Q., Jia, B.B., Xi, G., 2015. Experimental study on mean thrust of two plunging wings in tandem. AIAA J. 53 (6), 1693–1705.
Granlund, K.O., Ol, M.V., Bernal, L.P., 2013. Unsteady pitching flat plates. J. Fluid Mech. 733.
Gravish, N., Peters, J.M., Combes, S.A., Wood, R.J., 2015. Collective Flow enhancement by tandem flapping wings. Phys. Rev. Lett. 115 (18), 188101.
Green, M.A., Rowley, C.W., Smits, A.J., 2011. The unsteady three-dimensional wake produced by a trapezoidal pitching panel. J. Fluid Mech. 685, 117–145.
Griffith, M.D., Lo Jacono, D., Sheridan, J., Leontini, J.S., 2016. Passive heaving of elliptical cylinders with active pitching – from cylinders towards flapping foils. J. Fluids Struct. 67, 124–141.
Guo, X.X., Gao, Z., Yang, J.M., Moan, T., 2017. Hydrodynamic loads on a tidal turbine in random seas. In: Proceedings of the 12th European Wave and Tidal Energy Conference (EWTEC, August 27-September 2, Cork, Ireland.
Guo, X.X., Gao, Z., Yang, J.M., Moan, T., Lu, H.N., Li, X., Lu, W.Y., 2017. The effects of surface waves and submergence on the performance and loading of a tidal turbine. In: Proceedings of the ASME 36th International Conference on Ocean, Offshore and Arctic Engineering, OMAE2017-62233. June 25–30, Trondheim, Norway.
Guo, X.X., Gao, Z., Li, X., Yang, J.M., Moan, T., 2018. Loading and blade deflection of a tidal turbine in waves. J. Offshore Mech. Arct. Eng.
Guo, X.X., Yang, J.M., Gao, Z., Moan, T., Lu, H.N., 2018. The surface wave effects on the performance and the loading of a tidal turbine. Ocean Eng. 156, 120–134.
Gursul, I., Ho, C.M., 1992. High aerodynamic loads on an airfoil submerged in an unsteady stream. AIAA J. 30 (4), 1117–1119.
Harbig, R.R., Sheridan, J., Thompson, M.C., 2013. Reynolds number and aspect ratio effects on the leading-edge vortex for rotating insect wing planforms. J. Fluid Mech. 717, 166–192.
He, G.-Y., Wang, Q., Zhang, X., Zhang, S.-G., 2012. Numerical analysis on transitions and symmetry-breaking in the wake of a flapping foil. Acta Mech. Sin. 28 (6), 1551–1556.
Heathcote, S., Gursul, I., 2007. Flexible flapping airfoil propulsion at low Reynolds numbers. AIAA J. 45 (5), 1066–1079.
Heathcote, S., Martin, D., Gursul, I., 2004. Flexible flapping airfoil propulsion at zero freestream velocity. AIAA J. 42 (11), 2196–2204.
Heathcote, S., Wang, Z., Gursul, I., 2008. Effect of spanwise flexibility on flapping wing propulsion. J. Fluids Struct. 24 (2), 183–199.
Hejlesen, M.M., Koumoutsakos, P., Leonard, A., Walther, J.H., 2015. Iterative Brinkman penalization for remeshed vortex methods. J. Comput. Phys. 280, 547–562.
Hover, F.S., Haugsdal, Ø., Triantafyllou, M.S., 2004. Effect of angle of attack profiles in flapping foil propulsion. J. Fluids Struct. 19 (1), 37–47.
Hu, H., Ren, W., Liu, H., Wu, J., 2013. An experimental investigation on the asymmetric wake of an oscillating airfoil. In: 51st AIAA Aerospace Sciences Meeting Including the New Horizons Forum and Aerospace Exposition, p. 794.
Hutchinson, S.R., Brandner, P.A., Binns, J.R., Henderson, A.D., Walker, G.J., 2010. Development of a CFD model for an oscillating hydrofoil. In: Proceedings of the 17th Australasian Fluid Mechanics Conference; Auckland, New Zealand.
Jardin, T., Farcy, A., David, L., 2012. Three-dimensional effects in hovering flapping flight. J. Fluid Mech. 702, 102–125.
Jeanmonod, G., Olivier, M., 2017. Effects of chordwise flexibility on 2D flapping foils used as an energy extraction device. J. Fluids Struct. 70, 327–345.
Jones, K., Platzer, M., 1997. Numerical computation of flapping-wing propulsion and power extraction. In: Aiaa Aerospace Sciences Meeting and Exhibit.
Jones, K.D., Platzer, M.F., 1999. An experimental and numerical investigation of flapping-wing propulsion. In: AIAA Aerospace Sciences Meeting & Exhibit.
Jones, K.D., Dohring, C.M., Platzer, M.F., 1998. Experimental and computational investigation of the Knoller-Betz effect. AIAA J. 36 (7), 1240–1246.
Jones, K.D., Davids, S., Platzer, M.F., 1999. Oscillating-wing power generator. In: 3rd ASME/JSME Joint Fluids Engineering Conference.
Kang, C.K., Baik, Y.S., Bernal, L., Ol, M.V., Shyy, W., 2009. Fluid dynamics of pitching and plunging airfoils of Reynolds number between 1×10^4 and 6×10^4. In: AIAA Aerospace Sciences Meeting Including the New Horizons Forum and Aerospace Exposition.
Kang, C.K., Aono, H., Cesnik, C.E.S., Shyy, W., 2011. Effects of flexibility on the aerodynamic performance of flapping wings. J. Fluid Mech. 689, 32–74.
Karakas, F., Fenercioglu, I., 2016. Effect of side-walls on flapping-wing power-generation an experimental study. J. Appl. Fluid Mech. 9 (6), 2769–2779.
Karbasian, H.R., Esfahani, J.A., Barati, E., 2015. Simulation of power extraction from tidal currents by flapping foil hydrokinetic turbines in tandem formation. Renew. Energy 81, 816–824.
Katzmayr, R., 1922. Effect of Periodic Changes of Angle of Attack on Behavior of Airfoils. NACA Rept, vol. 147. Oct. (translated from Zeitschrift für Flugtechnik und Motorluftschiffahrt March 31, 1922, pp. 80–82, and April 13, 1922, pp. 95–101).
Kaya, M., Tuncer, I.H., 2007. Nonsinusoidal path optimization of a flapping airfoil. AIAA J. 45 (8), 2075–2082.
Khalid, M.S.U., Akhtar, I., Dong, H., Ahsan, N., 2015. Nonlinear characterization of flow over oscillating elliptic airfoils. In: Aiaa Aviation Conference, pp. 9–13.
Kim, D.H., Chang, J.W., 2010. Unsteady boundary layer for a pitching airfoil at low Reynolds numbers. J. Mech. Sci. Technol. 24 (1), 429–440.
Kim, D., Strom, B., Mandre, S., Breuer, K., 2017. Energy harvesting performance and flow structure of an oscillating hydrofoil with finite span. J. Fluids Struct. 70, 314–326.
Kinsey, T., Dumas, G., 2008. Parametric study of an oscillating airfoil in a power-extraction regime. AIAA J. 46 (6), 1318–1330.
Kinsey, T., Dumas, G., 2012. Optimal tandem configuration for oscillating-foils hydrokinetic turbine. J. Fluids Eng. 134 (3), 031103.
Knoller, R., 1909. Die Gesetze des Luftwiderstandes. Flug- und Motortechnik (Wien) 3 (21), 1–7.
Koochesfahani, M.M., 1989. Vortical patterns in the wake of an oscillating airfoil. AIAA J. 27 (9), 1200–1205.
Kumar, A.G., Hu, H., 2010. Flow structures in the wakes of tandem piezoelectric flapping wings. In: 28th AIAA Applied Aerodynamics Conference, p. 4939.
Kumar, R., Shin, H., 2019. Thrust estimation of a flapping foil attached to an elastic plate using multiple regression analysis. Int. J. Nav. Archit. Ocean Eng. 11 (2), 828–834.
Kuo, C.H., Hsieh, J.K., 2001. Unsteady flow structure and vorticity convections over the airfoil oscillating at high reduced frequency. Exp. Therm. Fluid Sci. 24 (3–4), 117–129.
Lahooti, M., Kim, D., 2019. Multi-body interaction effect on the energy harvesting performance of a flapping hydrofoil. Renew. Energy 130, 460–473.
Lai, J.C.S., Platzer, M.F., 1999. Jet characteristics of a plunging airfoil. AIAA J. 37 (12), 1529–1537.
Larsen, A., Walther, J.H., 1997. Aeroelastic analysis of bridge girder sections based on discrete vortex simulations. J. Wind Eng. Ind. Aerodyn. 67–68, 524–543.
Lee, T., Petrakis, G., Mokhtarian, F., Kafyeke, F., 2000. Boundary-Layer transition, separation, and reattachment on an oscillating airfoil. J. Aircr. 37 (2), 356–360.
Lee, J.S., Kim, C., Kim, K.H., 2006. Design of flapping airfoil for optimal aerodynamic performance in low-Reynolds number flows. AIAA J. 44 (9), 1960–1972.
Li, G.J., Lu, X.-Y., 2012. Force and power of flapping plates in a fluid. J. Fluid Mech. 712, 598–613.

Li, X., Liu, Y., Kou, J., Zhang, W., 2017. Reduced-order thrust modeling for an efficiently flapping airfoil using system identification method. J. Fluids Struct. 69, 137–153.
Lian, Y., Ol, M., Wei, S., 2008. Comparative Study of pitch-plunge airfoil aerodynamics at transitional Reynolds number. In: 46th AIAA Aerospace Sciences Meeting and Exhibit.
Liang, C., Ou, K., Premasuthan, S., Jameson, A., Wang, Z.J., 2011. High-order accurate simulations of unsteady flow past plunging and pitching airfoils. Comput. Fluid 40 (1), 236–248.
Lin, X., Wu, J., Zhang, T., 2019. Performance investigation of a self-propelled foil with combined oscillating motion in stationary fluid. Ocean Eng. 175, 33–49.
Ling, J., Kurzawski, A., Templeton, J., 2016. Reynolds averaged turbulence modelling using deep neural networks with embedded invariance. J. Fluid Mech. 807, 155–166.
Liu, H., Kawachi, K., 1998. A numerical study of insect flight. J. Comput. Phys. 146 (1), 124–156.
Liu, W., Xiao, Q., Cheng, F., 2013. A bio-inspired study on tidal energy extraction with flexible flapping wings. Bioinspiration Biomim. 8 (3), 036011.
Liu, W., Xiao, Q., Zhu, Q., 2016. Passive flexibility effect on oscillating foil energy harvester. AIAA J. 54 (4), 1172–1187.
Liu, Z., Qu, H., Shi, H., 2019. Numerical study on hydrodynamic performance of a fully passive flow-driven pitching hydrofoil. Ocean Eng. 177, 70–84.
Lu, K., Xie, Y.H., Zhang, D., 2013. Numerical study of large amplitude, nonsinusoidal motion and camber effects on pitching airfoil propulsion. J. Fluids Struct. 36, 184–194.
Lu, K., Xie, Y.H., Zhang, D., Lan, J.B., 2013. Numerical investigations into the asymmetric effects on the aerodynamic response of a pitching airfoil. J. Fluids Struct. 39, 76–86.
Lu, K., Xie, Y., Zhang, D., 2014. Nonsinusoidal motion effects on energy extraction performance of a flapping foil. Renew. Energy 64, 283–293.
Lu, K., Xie, Y., Zhang, D., Xie, G., 2015. Systematic investigation of the flow evolution and energy extraction performance of a flapping-airfoil power generator. Energy 89, 138–147.
Lua, K.B., Lim, T.T., Yeo, K.S., Oo, G.Y., 2007. Wake-structure formation of a heaving two-dimensional elliptic airfoil. AIAA J. 45 (7), 1571–1583.
Lua, K.B., Lim, T.T., Yeo, K.S., 2008. Aerodynamic forces and flow fields of a two-dimensional hovering wing. Exp. Fluid 45 (6), 1047–1065.
Lua, K.B., Lai, K.C., Lim, T.T., Yeo, K.S., 2010. On the aerodynamic characteristics of hovering rigid and flexible hawkmoth-like wings. Exp. Fluid 49 (6), 1263–1291.
Lua, K.B., Lim, T.T., Yeo, K.S., 2011. Effect of wing–wake interaction on aerodynamic force generation on a 2D flapping wing. Exp. Fluid 51 (1), 177–195.
Lua, K.B., Dash, S.M., Lim, T.T., Yeo, K.S., 2016. On the thrust performance of a flapping two-dimensional elliptic airfoil in a forward flight. J. Fluids Struct. 66, 91–109.
Mackowski, A.W., Williamson, C.H.K., 2015. Direct measurement of thrust and efficiency of an airfoil undergoing pure pitching. J. Fluid Mech. 765, 524–543.
Mackowski, A.W., Williamson, C.H.K., 2017. Effect of pivot location and passive heave on propulsion from a pitching airfoil. Phys. Rev. Fluid 2 (1).
Mantia, M.L., Dabnichki, P., 2013. Structural response of oscillating foil in water. Eng. Anal. Bound. Elem. 37 (6), 957–966.
Marais, C., Thiria, B., Wesfreid, J.E., Godoy-Diana, R., 2012. Stabilizing effect of flexibility in the wake of a flapping foil. J. Fluid Mech. 710, 659–669.
Martín-Alcántara, A., Fernandez-Feria, R., Sanmiguel-Rojas, E., 2015. Vortex flow structures and interactions for the optimum thrust efficiency of a heaving airfoil at different mean angles of attack. Phys. Fluids 27 (7), 073602.
Medjroubi, W., Stoevesandt, B., Carmo, B., Peinke, J., 2011. High-order numerical simulations of the flow around a heaving airfoil. Comput. Fluid 51 (1), 68–84.
Medjroubi, W., Stoevesandt, B., Peinke, J., 2012. Wake classification of heaving airfoils using the spectral/hp element method. J. Comput. Appl. Math. 236 (15), 3774–3782.
Miao, J.M., Ho, M.H., 2006. Effect of flexure on aerodynamic propulsive efficiency of flapping flexible airfoil. J. Fluids Struct. 22 (3), 401–419.
Monnier, B., Naguib, A.M., Koochesfahani, M.M., 2015. Influence of structural flexibility on the wake vortex pattern of airfoils undergoing harmonic pitch oscillation. Exp. Fluid 56 (4).
Moored, K.W., Dewey, P.A., Smits, A.J., Haj-Hariri, H., 2012. Hydrodynamic wake resonance as an underlying principle of efficient unsteady propulsion. J. Fluid Mech. 708, 329–348.
Moubogha, J.M., Ehrenstein, U., Astolfi, J.A., 2017. Forces on a pitching plate: an experimental and numerical study. Appl. Ocean Res. 69, 27–37.
Münch, C., Ausoni, P., Braun, O., Farhat, M., Avellan, F., 2010. Fluid–structure coupling for an oscillating hydrofoil. J. Fluids Struct. 26 (6), 1018–1033.
Muscutt, L.E., Weymouth, G.D., Ganapathisubramani, B., 2017. Performance augmentation mechanism of in-line tandem flapping foils. J. Fluid Mech. 827, 484–505.
Myose, R.Y., Iwata, J., 1996. Flow visualization of an oscillating airfoil with sawtooth trailing edge. AIAA J. 34 (8), 1748–1750.
Ohmi, K., Coutanceau, M., Loc, T.P., Dulieu, A., 1990. Vortex formation around an oscillating and translating airfoil at large incidences. J. Fluid Mech. 211 (-1), 37.
Ohmi, K., Coutanceau, M., Daube, O., Loc, T.P., 1991. Further experiments on vortex formation around an oscillating and translating airfoil at large incidences. J. Fluid Mech. 225 (-1), 607.
Ol, M.V., 2007. Vortical structures in high frequency pitch and plunge at low Reynolds number. In: AIAA Fluid Dynamics Conference and Exhibit.
Ol, M.V., Dong, H., Webb, C., 2008. Motion kinematics vs. angle of attack effects in high-frequency airfoil pitch/plunge. In: Fluid Dynamics Conference and Exhibit.
Olivier, M., Dumas, G., 2016. Effects of mass and chordwise flexibility on 2D self-propelled flapping wings. J. Fluids Struct. 64, 46–66.
Olivier, M., Dumas, G., 2016. A parametric investigation of the propulsion of 2D chordwise-flexible flapping wings at low Reynolds number using numerical simulations. J. Fluids Struct. 63, 210–237.
Pan, D., Deng, J., Shao, X., Liu, Z., 2016. On the propulsive performance of tandem flapping wings with a modified Immersed Boundary Method. Int. J. Comput. Methods 13 (05), 1650025.
Panah, A.E., Buchholz, J., 2012. Vortex Shedding and Wake Structure of a Plunging Wing. AIAA Aerospace Sciences Meeting Including the New Horizons Forum and Aerospace Exposition.
Panah, A.E., Buchholz, J.H.J., 2014. Parameter dependence of vortex interactions on a two-dimensional plunging plate. Exp. Fluid 55 (3).
Panah, A.E., Akkala, J., Buchholz, J., 2013. Vortex Dynamics of a Finite-Aspect-Ratio Plunging Wing. AIAA Aerospace Sciences Meeting Including the New Horizons Forum and Aerospace Exposition.
Parker, K., von Ellenrieder, K.D., Soria, J., 2007. Morphology of the forced oscillatory flow past a finite-span wing at low Reynolds number. J. Fluid Mech. 571, 327.
Pedro, G., Suleman, A., Djilali, N., 2003. A numerical study of the propulsive efficiency of a flapping hydrofoil. Int. J. Numer. Methods Fluids 42 (5), 493–526.
Peng, J., Chen, G.S., 2012. Flow-oscillating structure interactions and the applications to propulsion and energy harvest. Appl. Phys. Res. 4 (2).
Peng, Z.R., Huang, H.B., Lu, X.Y., 2018. Collective locomotion of two closely spaced self-propelled flapping plates. J. Fluid Mech. 849, 1068–1095.
Peng, Z.R., Huang, H.B., Lu, X.Y., 2018. Hydrodynamic schooling of multiple self-propelled flapping plates. J. Fluid Mech. 853, 587–600.
Platzer, M.F., Ashraf, M.A., Young, J., Lai, J.C.S., 2010. Extracting power in jet streams_ pushing the performance of flapping wing technology. In: Congress of the International Council of the Aeronautical Sciences, pp. 961–970.
Politis, G.K., 2004. Simulation of unsteady motion of a propeller in a fluid including free wake modeling. Eng. Anal. Bound. Elem. 28 (6), 633–653.
Politis, G.K., 2009. A BEM code for the calculation of flow around systems of independently movingbodies including free shear layer dynamics. In: Sapountzakis, E.J., Aliabadi, M.H. (Eds.), Advances in Boundary Element Techniques X, Athens, Greece, pp. 381–388.
Politis, G.K., 2011. Application of a BEM time stepping algorithm in understanding complex unsteady propulsion hydrodynamic phenomena. Ocean Eng. 38 (4), 699–711.
Politis, G., Politis, K., 2014. Biomimetic propulsion under random heaving conditions, using active pitch control. J. Fluids Struct. 47, 139–149.
Politis, G.K., Tsarsitalidis, V.T., 2009. Simulating biomimetic (flapping foil) flows for comprehension, reverse engineering and design. In: First International Symposium on Marine Propulsors, SMP'09, Trondheim, Norway.
Politis, G.K., Tsarsitalidis, V.T., 2013. Biomimetic propulsion using twin oscillating wings. In: Third International Symposium on Marine Propulsors, SMP'13, Tasmania, Australia.
Politis, G.K., Tsarsitalidis, V.T., 2014. Flapping wing propulsor design: an approach based on systematic 3D-BEM simulations. Ocean Eng. 84, 98–123.
Prempraneerach, P., Hover, F.S., Triantafyllou, M.S., 2003. The effect of chordwise flexibility on the thrust and efficiency of a flapping foil. In: Proceedings of 13th International Symposium Unmanned Untethered Submersible Technology, pp. 1–10.
Quinn, D.B., Lauder, G.V., Smits, A.J., 2015. Maximizing the efficiency of a flexible propulsor using experimental optimization. J. Fluid Mech. 767, 430–448.
Raissi, M., Wang, Z., Triantafyllou, M.S., Karniadakis, G.E., 2019. Deep learning of vortex-induced vibrations. J. Fluid Mech. 861, 119–137.
Ramamurti, R., Sandberg, W., 2001. Simulation of flow about flapping airfoils using finite element incompressible flow solver. AIAA J. 39 (2), 253–260.
Rasmussen, J.T., Hejlesen, M.M., Larsen, A., Walther, J.H., 2010. Discrete vortex method simulations of the aerodynamic admittance in bridge aerodynamics. J. Wind Eng. Ind. Aerodyn. 98 (12), 754–766.
Read, D.A., Hover, F.S., Triantafyllou, M.S., 2003. Forces on oscillating foils for propulsion and maneuvering. J. Fluids Struct. 17 (1), 163–183.
Rivera, M., Vorobieff, P., Ecke, R.E., 1998. Turbulence in flowing soap films: velocity, vorticity, and thickness fields. Phys. Rev. Lett. 81 (7), 1417–1420.
Rostami, A.B., Armandei, M., 2017. Renewable energy harvesting by vortex-induced motions: review and benchmarking of technologies. Renew. Sustain. Energy Rev. 70, 193–214.
Rozhdestvensky, K.V., Ryzhov, V.A., 2003. Aerohydrodynamics of flapping-wing propulsors. Prog. Aerosp. Sci. 39 (8), 585–633.
Sadeghi, H., Mani, M., 2009. Investigation of flow field behind an oscillating airfoil below and beyond static stall. World Conference on. Exp. Heat Trans., Fluid Mechan. Thermodyn. 58, 353–354.
Sadeghi, H., Mani, M., Ardakani, M.A., 2011. Effect of amplitude and mean angle of attack on wake of an oscillating airfoil. World Acad. Sci., Eng. Technol. 23, 125–129.
Sadeghi, H., Mani, M., Alighanbari, H., 2015. An experimental study of the unsteady wake of an Eppler-361 airfoil. In: Fluid Dynamics Conference and Exhibit.
Sarkar, S., Singasani, V., 2009. Comparison of fundamental flapping kinematics of an airfoil. In: 39th AIAA Fluid Dynamics Conference; San Antonio, Texas.
Schnipper, T., Andersen, A., Bohr, T., 2009. Vortex wakes of a flapping foil. J. Fluid Mech. 633, 411.
Schouveiler, L., Hover, F.S., Triantafyllou, M.S., 2005. Performance of flapping foil propulsion. J. Fluids Struct. 20 (7), 949–959.
Shao, X., Pan, D., Deng, J., Yu, Z., 2010. Numerical studies on the propulsion and wake structures of finite-span flapping wings with different aspect ratios. J. Hydrodyn., Ser. B 22 (2), 147–154.
Shin, S., Bae, S.Y., Kim, I.C., Kim, Y.J., 2009. Effects of flexibility on propulsive force acting on a heaving foil. Ocean Eng. 36 (3–4), 285–294.

Shinde, S.Y., Arakeri, J.H., 2013. Jet meandering by a foil pitching in quiescent fluid. Phys. Fluids 25 (4), 041701.
Simpson, B.J., Hover, F.S., Triantafyllou, M.S., 2008. Experiments in direct energy extraction through flapping foils. In: Proceedings of the Eighteenth International Offshore and Polar Engineering Conference.
Sitorus, P.E., Ko, J.H., 2019. Power extraction performance of three types of flapping hydrofoils at a Reynolds number of 1.7 E6. Renew. Energy 132, 106–118.
Smits, A.J., 2019. Undulatory and oscillatory swimming. J. Fluid Mech. 874.
Srigrarom, S., Chai, W.S., 2009. Optimization of SD7003 & SD8020 foils oscillating motions for propulsion. In: 27th AIAA Applied Aerodynamics Conference.
Srigrarom, S., Vincent, C., 2008. Effect of Pitching and Heaving Motions of SD8020 Hydrofoil on Thrust and Efficiency for Swimming Propulsion. APS Division of Fluid Dynamics Meeting. APS Division of Fluid Dynamics Meeting Abstracts.
Taira, K., Colonius, T.I.M., 2009. Three-dimensional flows around low-aspect-ratio flat-plate wings at low Reynolds numbers. J. Fluid Mech. 623, 187.
Tay, W.B., Lim, K.B., 2010. Numerical analysis of active chordwise flexibility on the performance of non-symmetrical flapping airfoils. J. Fluids Struct. 26 (1), 74–91.
Teng, L., Deng, J., Pan, D., Shao, X., 2016. Effects of non-sinusoidal pitching motion on energy extraction performance of a semi-active flapping foil. Renew. Energy 85, 810–818.
Thaweewat, N., Bos, F.M., van Oudheusden, B.W., Bijl, H., 2009. Numerical study of vortex-wake interactions and performance of a two-dimensional flapping foil. In: 47th AIAA Aerospace Sciences Meeting Including The New Horizons Forum and Aerospace Exposition, p. 791.
Thaweewat, N., Phoemsapthawee, S., Juntasaro, V., 2018. Semi-active flapping foil for marine propulsion. Ocean Eng. 147, 556–564.
Tian, W., Bodling, A., Liu, H., Wu, J.C., He, G., Hu, H., 2016. An experimental study of the effects of pitch-pivot-point location on the propulsion performance of a pitching airfoil. J. Fluids Struct. 60, 130–142.
Tian, R., Mitchell, R., Martin-Alarcon, L., Shu, F., 2013. Experimental investigation of 2D flexible plunging hydrofoil. J. Flow Vis. Image Process. 20 (4), 243–260.
Tian, X., Tao, L., Li, X., Yang, J., 2017. Hydrodynamic coefficients of oscillating flat plates at 0.15 KC 3.15. J. Mar. Sci. Technol. 22 (1), 101–113.
Tian, X., Xiao, L., Zhang, X., Yang, J., Tao, L., Yang, D., 2017. Flow around an oscillating circular disk at low to moderate Reynolds numbers. J. Fluid Mech. 812, 1119–1145.
Torres, G.E., Mueller, T.J., 2004. Low aspect ratio aerodynamics at low Reynolds numbers. AIAA J. 42 (5), 865–873.
Triantafyllou, M.S., Triantafyllou, G.S., Gopalkrishnan, R., 1991. Wake mechanics for thrust generation in oscillating foils. Phys. Fluids A Fluid Dyn. 3 (12), 2835–2837.
Tsarsitalidis, V., Politis, G., 2015. Simulating Biomimetic Propulsors under spring loading and/or active control for the pitching motion of the wings. In: Proceedings of Fourth International Symposium on Marine Propulsors, SMP'15, Austin, Texas, USA.
Tuncer, I.H., Kaya, M., 2005. Optimization of flapping airfoils for maximum thrust and propulsive efficiency. AIAA J. 43 (11), 2329–2336.
Van Buren, T., Floryan, D., Quinn, D., Smits, A.J., 2017. Nonsinusoidal gaits for unsteady propulsion. Phys. Rev. Fluid 2 (5).
Visbal, M.R., 2009. High-fidelity simulation of transitional flows past a plunging airfoil. AIAA J. 47 (47), 2685–2697.
Visbal, M.R., Shang, J.S., 1989. Investigation of the flow structure around a rapidly pitching airfoil. AIAA J. 27 (8), 1044–1051.
Visbal, M., Yilmaz, T.O., Rockwell, D., 2013. Three-dimensional vortex formation on a heaving low-aspect-ratio wing: computations and experiments. J. Fluids Struct. 38, 58–76.
von Ellenrieder, K.D., Pothos, S., 2007. PIV measurements of the asymmetric wake of a two dimensional heaving hydrofoil. Exp. Fluid 44 (5), 733–745.
von Ellenrieder, K.D., Parker, K., Soria, J., 2001. Visualization of a three dimensional heaving aerofoil flow. In: 14th Australasian Fluid Mechanics Conference.
von Ellenrieder, K.D., Parker, K., Soria, J., 2002. Visualization of the three dimensional flow behind oscillating foils. AIAA Aerospace Sci. Meeting Exhibit.
von Ellenrieder, K.D., Parker, K., Soria, J., 2003. Flow structures behind a heaving and pitching finite-span wing. J. Fluid Mech. 490, 129–138.
von Kármán, T., Burgers, J.M., 1943. In: Durand, W.F., Division, E. (Eds.), General Aerodynamic Theory—Perfect Fluids. Aerodynamic Theory, vol. 2. Julius–Springer, Berlin, p. 308.
Walther, J.H., Larsen, A., 1997. Two dimensional discrete vortex method for application to bluff body aerodynamics. J. Wind Eng. Ind. Aerodyn. 67–68, 183–193.
Wan, Z.Y., Sapsis, T.P., 2018. Machine learning the kinematics of spherical particles in fluid flows. J. Fluid Mech. 857.
Wang, Q., Goosen, J.F.L., van Keulen, F., 2016. A predictive quasi-steady model of aerodynamic loads on flapping wings. J. Fluid Mech. 800, 688–719.
Wang, S., He, G., Zhang, X., 2016. Self-propulsion of flapping bodies in viscous fluids: recent advances and perspectives. Acta Mech. Sin. 32 (6), 980–990.
Wang, Y., Sun, X., Huang, D., Zheng, Z., 2016. Numerical investigation on energy extraction of flapping hydrofoils with different series foil shapes. Energy 112, 1153–1168.
Wang, Z., Du, L., Zhao, J., Sun, X., 2017. Structural response and energy extraction of a fully passive flapping foil. J. Fluids Struct. 72, 96–113.
Wang, Y., Huang, D., Han, W., YangOu, C., Zheng, Z., 2017. Research on the mechanism of power extraction performance for flapping hydrofoils. Ocean Eng. 129, 626–636.
Wang, P., Tian, X., Lu, W., Hu, Z., Luo, Y., 2019. Dynamic modeling and simulations of the wave glider. Appl. Math. Model. 66, 77–96.
Wen, B., Tian, X., Dong, X., Peng, Z., Zhang, W., 2017. Influences of surge motion on the power and thrust characteristics of an offshore floating wind turbine. Energy 141, 2054–2068.
Wen, B., Wei, S., Wei, K., Yang, W., Peng, Z., Chu, F., 2017. Power fluctuation and power loss of wind turbines due to wind shear and tower shadow. Front. Mechan. Eng. 12 (3), 1–12.
Wen, B., Dong, X., Tian, X., Peng, Z., Zhang, W., Wei, K., 2018. The power performance of an offshore floating wind turbine in platform pitching motion. Energy 154, 508–521.
Wen, B., Tian, X., Dong, X., Peng, Z., Zhang, W., 2018. On the power coefficient overshoot of an offshore floating wind turbine in surge oscillations. Wind Energy 21 (11), 1076–1091.
Wood, C.J., Kirmani, S.F.A., 1970. Visualization of heaving aerofoil wakes including the effect of a jet flap. J. Fluid Mech. 41 (03), 627.
Wu, T.Y., 2010. A review on fish swimming and bird/insect flight. Annu. Rev. Fluid Mech. 43 (1).
Wu, J., Qiu, Y.L., Shu, C., Zhao, N., 2014. Pitching-motion-activated flapping foil near solid walls for power extraction: a numerical investigation. Phys. Fluids 26 (8), 083601.
Wu, J., Chen, Y.L., Zhao, N., 2015. Role of induced vortex interaction in a semi-active flapping foil based energy harvester. Phys. Fluids 27 (9), 093601.
Wu, J., Shu, C., Zhao, N., Tian, F.B., 2015. Numerical study on the power extraction performance of a flapping foil with a flexible tail. Phys. Fluids 27 (1), 013602.
Wu, J., Wu, J., Tian, F.B., Zhao, N., Li, Y.D., 2015. How a flexible tail improves the power extraction efficiency of a semi-activated flapping foil system: a numerical study. J. Fluids Struct. 54, 886–899.
Wu, J., Chen, Y., Zhao, N., Wang, T., 2016. Influence of stroke deviation on the power extraction performance of a fully-active flapping foil. Renew. Energy 94, 440–451.
Xiao, Q., Liao, W., 2009. Numerical study of asymmetric effect on a pitching foil. Int. J. Mod. Phys. C 20 (10), 1663–1680.
Xiao, Q., Liao, W., 2010. Numerical investigation of angle of attack profile on propulsion performance of an oscillating foil. Comput. Fluid 39 (8), 1366–1380.
Xiao, Q., Zhu, Q., 2014. A review on flow energy harvesters based on flapping foils. J. Fluids Struct. 46, 174–191.
Xiao, Q., Liao, W., Yang, S., Peng, Y., 2012. How motion trajectory affects energy extraction performance of a biomimic energy generator with an oscillating foil? Renew. Energy 37 (1), 61–75.
Xie, Y., Lu, K., Zhang, D., 2014. Investigation on energy extraction performance of an oscillating foil with modified flapping motion. Renew. Energy 63, 550–557.
Xu, J., Sun, H., 2016. Experimental studies of passive oscillating hydrofoil for tidal current energy extracting. J. Harbin Eng. Univ. 37 (2), 248–253.
Yang, J., Tian, X., Li, X., 2014. Hydrodynamic characteristics of an oscillating circular disk under steady in-plane current conditions. Ocean Eng. 75, 53–63.
Yilmaz, T.O., Rockwell, D., 2012. Flow structure on finite-span wings due to pitch-up motion. J. Fluid Mech. 691, 518–545.
Young, J., Lai, J.C.S., 2004. Oscillation frequency and amplitude effects on the wake of a plunging airfoil. AIAA J. 42 (10), 2042–2052.
Young, J., Lai, J.C.S., 2007. Vortex lock-in phenomenon in the wake of a plunging airfoil. AIAA J. 45 (2), 485–490.
Young, J., Lai, J.C.S., 2014. Effect of angle of attack kinematics on passive flapping foil power generation. In: Congress of the International Council of the Aeronautical Sciences.
Young, J., Lai, J.C.S., Platzer, M.F., 2014. A review of progress and challenges in flapping foil power generation. Prog. Aerosp. Sci. 67, 2–28.
Young, J.D., Morris, S.E., Schutt, R.R., Williamson, C.H.K., 2019. Effect of hybrid-heave motions on the propulsive performance of an oscillating airfoil. J. Fluids Struct. 89, 203–218.
Ysasi, A., Kanso, E., Newton, P.K., 2011. Wake structure of a deformable Joukowski airfoil. Phys. D Nonlinear Phenom. 240 (20), 1574–1582.
Yu, M.L., Hu, H., Wang, Z.J., 2012. Experimental and numerical investigations on the asymmetric wake vortex structures around an oscillating airfoil. Tech. Report Ieice Sdm 108 (236), 1–6.
Yu, M.L., Wang, Z.J., Hu, H., 2013. High fidelity numerical simulation of airfoil thickness and kinematics effects on flapping airfoil propulsion. J. Fluids Struct. 42, 166–186.
Yu, D., Sun, X., Bian, X., Huang, D., Zheng, Z., 2017. Numerical study of the effect of motion parameters on propulsive efficiency for an oscillating airfoil. J. Fluids Struct. 68, 245–263.
Zaman, R.I., Lai, J., Young, J., Ashraf, M., 2014. Comparison study of non sinusoidal pitch over sinusoidal pitch at higher angle of attack. AIAA Appl. Aerodyn. Conf. 129–130.
Zhang, J., 2017. Footprints of a flapping wing. J. Fluid Mech. 818, 1–4.
Zhang, J., Childress, S., Libchaber, A., Shelley, M., 2000. Flexible filaments in a flowing soap film as a model for one-dimensional flags in a two-dimensional wind. Nature 408, 835–839.
Zheng, Z.C., Wei, Z., 2012. Study of mechanisms and factors that influence the formation of vortical wake of a heaving airfoil. Phys. Fluids 24 (10), 103601.
Zhu, Q., 2007. Numerical simulation of a flapping foil with chordwise or spanwise flexibility. AIAA J. 45 (10), 2448–2457.
Zhu, Q., 2011. Optimal frequency for flow energy harvesting of a flapping foil. J. Fluid Mech. 675, 495–517.
Zhu, Q., 2012. Energy harvesting by a purely passive flapping foil from shear flows. J. Fluids Struct. 34, 157–169.
Zhu, Q., Haase, M., Wu, C.H., 2009. Modeling the capacity of a novel flow-energy harvester. Appl. Math. Model. 33 (5), 2207–2217.
Zhu, X., He, G., Zhang, X., 2014. How flexibility affects the wake symmetry properties of a self-propelled plunging foil. J. Fluid Mech. 751, 164–183.

Zhu, X., He, G., Zhang, X., 2014. Numerical study on hydrodynamic effect of flexibility in a self-propelled plunging foil. Comput. Fluid 97, 1–20.
Zhu, B., Han, W., Sun, X., Wang, Y., Cao, Y., Wu, G., Huang, D., Zheng, Z.C., 2015. Research on energy extraction characteristics of an adaptive deformation oscillating-wing. J. Renew. Sustain. Energy 7 (2), 023101.
Zhu, Q., Wolfgang, M.J., Yue, D.K.P., Triantafyllou, M.S., 2002. Three-dimensional flow structures and vorticity control in fish-like swimming. J. Fluid Mech. 468, 1–28.